CHANDRA AND XMM-NEWTON OBSERVATIONS OF A SAMPLE OF LOW-REDSHIFT FRI AND FRII RADIO-GALAXY NUCLEI

D. A. Evans[1,2], D. M. Worrall[1], M. J. Hardcastle[3], R. P. Kraft[2], M. Birkinshaw[1]

ABSTRACT

We present spectral results, from *Chandra* and *XMM-Newton* observations, of a sample of 22 low-redshift ($z < 0.1$) radio galaxies, and consider whether the core emission originates from the base of a relativistic jet, an accretion flow, or contains contributions from both. We find correlations between the unabsorbed X-ray, radio, and optical fluxes and luminosities of FRI-type radio-galaxy cores, implying a common origin in the form of a jet. On the other hand, we find that the X-ray spectra of FRII-type radio-galaxy cores is dominated by absorbed emission, with $N_{\rm H} \gtrsim 10^{23}$ atoms cm^{-2}, that is likely to originate in an accretion flow. We discuss several models which may account for the different nuclear properties of FRI- and FRII-type cores, and also demonstrate that both heavily obscured, accretion-related, and unobscured, jet-related components may be present in all radio-galaxy nuclei. Any absorbed, accretion-related, components in FRI-type galaxies have low radiative efficiencies.

Subject headings: galaxies: active - galaxies: jets - X-rays: galaxies

1. INTRODUCTION

The physical origin of X-ray emission in the nuclei of radio galaxies is a topic of considerable debate. It is unclear whether the emission primarily originates in an accretion flow, or instead has an origin associated with a parsec-scale radio jet. The evidence in favor of each interpretation provides motivation to this paper, which uses spectroscopy of the X-ray cores to distinguish the two possibilities. On the one hand, it has been suggested

[1]University of Bristol, Department of Physics, Tyndall Avenue, Bristol BS8 1TL, UK

[2]Harvard-Smithsonian Center for Astrophysics, 60 Garden Street, Cambridge, MA 02138, USA

[3]School of Physics, Astronomy & Mathematics, University of Hertfordshire, College Lane, Hatfield, AL10 9AB, UK

that at least a fraction of the nuclear X-ray emission of radio galaxies has an origin at the unresolved base of a parsec-scale radio jet (e.g., Fabbiano et al. 1984). The best pieces of evidence in favor of this hypothesis are the observed correlations between the *ROSAT* X-ray and VLA radio core fluxes and luminosities measured in the B2 (Canosa et al. 1999) and 3CRR (Hardcastle & Worrall 1999) samples, supporting a nuclear jet-related origin for at least the soft X-ray emission. Hardcastle & Worrall (1999) demonstrated that, since the jet-generated radio emission is believed to be strongly affected by relativistic beaming, the flux–flux and luminosity–luminosity correlations would have considerable intrinsic scatter if the X-ray emission were instead to originate in an isotropic accretion flow.

Further constraints on the physical processes present in radio-galaxy nuclei come from *HST* observations (Chiaberge et al. 1999; Hardcastle & Worrall 2000). Correlations are observed between the radio and optical luminosities of 3CR FRI-type nuclei, again supporting a common origin at the base of a parsec-scale jet. However, FRII-type nuclei show a range of behavior at optical wavelengths: those sources with weak or narrow optical line-emission lie on the (presumably jet-related) radio–optical luminosity–luminosity correlation established for the FRI-type sources (Chiaberge et al. 2000). However, the optical luminosities of broad-line FRII-type sources lie significantly above this trendline, and Chiaberge et al. (2000) interpret these sources as being oriented to the observer such that significant optical emission from an accretion disk is observed, consistent with predictions from AGN-unification schemes (e.g., Antonucci 1993; Urry & Padovani 1995). Additional evidence in favor of jet-related X-ray emission in the nuclei of radio galaxies is found when considering the multiwavelength spectral energy distributions (SED) of these sources. As demonstrated by Capetti et al. (2002), Chiaberge et al. (2003), and Pellegrini et al. (2003), the nuclear SED of certain FRI-type radio galaxies may be modeled by synchrotron and synchrotron self-Compton emission from the base of a relativistic jet.

There is, however, an alternative interpretation of the origin of nuclear X-ray emission: that it is emission from an accretion flow. Observations in favor of this model include the detection of broadened Fe Kα lines and short-timescale ($\sim$ks) variability, both of which were used to argue for a physical origin in the inner regions of an accretion flow (Gliozzi et al. 2003, 2004). In a recent study of a sample of FRI-type radio-galaxy nuclei, Donato et al. (2004) showed that several sources with strong optical jet emission are not accompanied by strong X-ray emission, which may suggest a different physical origin for the two. Further, Merloni et al. (2003) argued that the observed correlations between the luminosities of radio and X-ray emission in radio-galaxy cores may be part of a 'fundamental plane', linking the radio and X-ray emission with black hole mass in both radio-loud and radio-quiet AGN. They suggest that the X-ray emission in all these sources has an origin in the form of an accretion flow, although they cannot rule out a significant contribution from the jet to the

X-ray emission of the radio-loud sources.

In addition to the debate surrounding the origin of the X-ray emission, there has been some controversy over whether physical differences exist in the accretion-flow modes of FRI- and FRII-type sources, and over the presence and rôle of obscuring tori in these sources. It is unclear whether the Fanaroff-Riley dichotomy observed on large (kpc–Mpc) scales (Fanaroff & Riley 1974) is due to the primarily *extrinsic* impact of the hot-gas environment on the jet propagating through it (e.g., Bicknell 1994, 1995; Gopal-Krishna & Wiita 2000), or rather ensues from *intrinsic* differences in the structure of the accretion flow and/or torus (see discussion by Gopal-Krishna & Wiita 2000). There is growing evidence (e.g., Reynolds et al. 1996; Donato et al. 2004) to suggest that FRI-type radio-galaxy nuclei possess radiatively inefficient, possibly advection-dominated (e.g., Narayan & Yi 1995) accretion flows, rather than standard, geometrically thin disks. It has also been claimed from the low intrinsic absorption measured at X-ray wavelengths (Donato et al. 2004), together with the high optical-core detection rate (Chiaberge et al. 1999), that an obscuring torus, required by AGN-unification schemes, is *absent* in FRI-type radio galaxies. However, as noted by Hardcastle et al. (2002), Worrall et al. (2003), and Cao & Rawlings (2004), if the optical and X-ray emission is dominated by a jet and occurs on scales larger that of a torus, then one cannot comment directly on the presence or absence of the torus using the X-ray absorption and optical reddening properties alone.

As the orientation-dependent effects of relativistic beaming and the putative obscuring torus are expected to play a large part in determining the observed properties of a radio-galaxy nucleus, it is important to select sources based on their low-frequency (and hence isotropic) emission characteristics, such as in the 3C and 3CRR samples. In this paper, we present the results of a *Chandra* and *XMM-Newton* spectral analysis of a sample of the nuclei of 22 radio galaxies at $z < 0.1$, 19 of which are from the 3CRR catalogue, with the remaining sources, 3C 403, 3C 405 (Cygnus A), and Centaurus A, included due to their high quality spectra. The high spatial resolution of *Chandra* means that it is possible to disentangle confusing kpc-scale jet emission from that of the core, while the large collecting area of *XMM-Newton* allows tight constraints to be placed on spectral parameters. Each observatory covers a sufficiently large energy range that both soft unobscured X-ray emission and hard obscured emission, possibly viewed through a torus, may be observed, providing direct tests of AGN-unification models.

This paper is organized as follows. Section 2 contains a description of the data and a summary of their analysis. The results from fitting the spectra of the nuclei of each source are presented in Section 3. In Section 4, we discuss the X-ray, radio, and optical flux and luminosity correlations. In Section 5, we discuss the presence that an obscuring torus is

present in FRI-type radio galaxies, while in Section 6 we interpret the observed differences in the X-ray nuclei of FRI- and FRII-type sources. We end with our conclusions in Section 7. All results presented in this paper use a cosmology in which $\Omega_{\rm m,0} = 0.3$, $\Omega_{\Lambda,0} = 0.7$, and $\rm H_0 = 70$ km s^{-1} Mpc^{-1}. When distinguishing between different model fits to the data, we present F-statistic results, although we note that this method may be unreliable in such circumstances (Protassov et al. 2002). We adopt thresholds of 95 and 99.9 per cent for marginally and highly significant improvements in the fit, respectively. Errors quoted in this paper are 90 per cent confidence for one parameter of interest (i.e., $\chi^2_{\rm min} + 2.7$), unless otherwise stated.

2. OBSERVATIONS AND ANALYSIS

Out of a total of 35 radio galaxies at $z < 0.1$ in the 3CRR catalogue (excluding the starburst galaxy 3C 231), 19 have been observed with *Chandra* or *XMM-Newton*. In total, 16 *Chandra* and 5 *XMM-Newton* observations of the sources are available at the time of writing, with the majority taken from the public data archives, together with some proprietary GO and GTO data. We compare results with those for Centaurus A (Evans et al. 2004), 3C 403 (Kraft et al. 2005), and 3C 405 (Cygnus A). Centaurus A is the nearest and best-studied AGN, while 3C 403 and 3C 405 are nearby FRII-type sources, and so each provides a useful comparison with the other sources in our sample. The main properties of the sources, including their redshift, Fanaroff-Riley classification, optical source type [Low-Excitation Radio Galaxy (LERG), Narrow-Line Radio Galaxy (NLRG), or Broad-Line Radio Galaxy (BLRG)], and V-band apparent magnitude, are given in Table 1. The redshifts quoted are taken from the online 3CRR catalogue[1], compiled by M. J. Hardcastle based on data from Laing et al. (1983) and with updates collated by Laing, Riley, and Hardcastle. The classification of the excitation properties of the sources follows Laing et al. (1994) and Jackson & Rawlings (1997), who define high-excitation objects as having [OIII]/H$\alpha > 0.2$ and equivalent widths of [OIII] > 3Å.

The *Chandra* data were reprocessed using CIAO v3.1 with the CALDB v2.2.8 calibration database to create a new level 2 events file with grades 0, 2, 3, 4, 6, afterglow events preserved, and the 0.5-arcsec pixel randomization removed. To check for intervals of high particle background, light curves were extracted for the chip upon which the source was located, excluding the source itself and any other noticeable point sources. The light curves were filtered based on the 3σ-clipping method of the user-contributed ANALYZE_LTCRV script,

[1]http://www.3crr.dyndns.org/

available from the CXC website[2].

The *XMM-Newton* data were reprocessed using SAS version 5.4.1, and calibrated event files were generated using the EMCHAIN and EPCHAIN scripts, with the additional filtering criteria of selecting events with only the PATTERN≤4 and FLAG=0 attributes. Periods of high particle background were screened by extracting light curves from the whole field of view, excluding a circle centered on the source, and selecting only events with PATTERN=0 and FLAG=0 attributes and for an energy range of 10–12 keV (MOS) cameras and 12–14 keV (pn).

For the analysis of nuclear emission, it is important to minimize the contribution of contaminating extended emission to the nuclear spectrum, meaning that *Chandra* observations of the sources are desirable. We extract on-source spectra from a small-radius circle (typically 2.5 pixels or 1.23″ in the case of *Chandra*, and 35″ in the case of *XMM-Newton*) and use local background subtraction. We take care to exclude unrelated contaminating sources and resolved kiloparsec-scale jet emission. The fluxes and luminosities quoted in this paper are corrected for the (generally small - typically ∼10–15%) fraction of missing counts that are the result of using a small aperture and the local background subtraction.

Spectra were extracted and calibration files generated using the standard CIAO and SAS scripts, PSEXTRACT and EVSELECT, respectively. Spectral fitting was performed on data grouped to a minimum of 25 counts per bin over an energy range 0.5–7 keV (*Chandra*) and 0.5–10 keV (*XMM-Newton*). Models were fitted to the background-subtracted source spectra, increasing in complexity until an adequate fit was achieved. In cases where two components of similar power-law spectral indices but different absorptions give the best fit to a spectrum, we cannot rule out the alternative of a single power-law index and a range of absorptions. The results of the spectral fitting were checked for their consistency, either by comparing them with previously published work, or, where possible, by intercomparing results from *Chandra* and *XMM-Newton*. In cases where the addition of a small-scale thermal component to the nuclear spectra of *Chandra* data was necessary, a consistency check was performed between the numbers of thermal counts found spectrally and extended counts found spatially via fitting a point source and β-model convolved with the PSF to the radial surface-brightness profile.

Pileup can be a concern when analyzing the X-ray spectrum of even a moderately bright point source, especially with *Chandra* data. A consideration of the count rates and an inspection of the spatial distribution of *Chandra* images filtered solely for 'afterglow' events (see discussion by Evans et al. 2005) showed that observations of three sources, Centaurus A,

[2]http://cxc.harvard.edu

NGC 6251 and 3C 390.3, are significantly affected by pileup (pileup fraction > 10%). The piled spectrum of Centaurus A is extensively discussed by Evans et al. (2004). The nuclear spectrum of NGC 6251 may be recovered by using an annular extraction region and therefore sampling only the wings of the PSF (Evans et al. 2005). For 3C 390.3, the source flux is sufficiently high that the nuclear spectrum of the source may be extracted from the frame transfer streak, using the method of Marshall et al. (2005) to correct for the fraction of events that occurred in the frame transfer streak.

3. RESULTS

In Table 3, we give the results of our analyses of each source. It is clear that no single model provides an adequate fit to every spectrum, with some sources having essentially no intrinsic absorption, and others having absorbing columns in excess of 10^{23} atoms cm^{-2}, together with fluorescent Fe Kα line-emission. We note that thermal emission from an extended component is sometimes not fully subtracted by local background subtraction. A range of power-law indices is also observed: best-fitting values range from 1.47 to 2.37. Further, the 2–10 keV intrinsic (unabsorbed) luminosities of the primary power law components span five orders of magnitude, with values ranging from 2×10^{39} to 3×10^{44} ergs s^{-1}. Again, we note that for spectra for which the best fitting model is two components of similar power-law spectral indices but different absorptions, we cannot rule out the alternative of a single power-law index and a range of absorptions.

In Table 4, we show the intrinsic absorption and unabsorbed 1-keV flux and luminosity densities of each X-ray spectral power-law component in the best-fit model for the sources. In addition, we give the flux and luminosity densities of the unresolved cores of each source, measured at 5 GHz with the VLA and with *HST* at red wavelengths (typically using the F702W filter). The 5-GHz VLA flux and luminosity densities are taken from the online 3CRR catalogue[3] and references therein. The majority of the *HST* optical values are taken from Hardcastle & Worrall (2000), who extracted the unresolved core flux densities from circular extraction regions centered on the source. The *HST* values are dereddened for Galactic absorption only. These values were checked for their consistency in an independent analysis (O. Shorttle, private communication), and in several cases this analysis provided values for sources not studied by Hardcastle & Worrall (2000). An independent analysis of the optical nuclei of radio galaxies sources was performed by Chiaberge et al. (1999); the values we quote in this paper generally agree with those of Chiaberge et al. (1999) to

[3]http://www.3crr.dyndns.org/

within a factor of 2, which is reasonable given the systematic uncertainties in background subtraction. Not all sources whose X-ray spectra we have analyzed have accompanying *HST* observations, either due to them not being observed, or due to other complications, such as the presence of foreground stars, or the mispointing of the telescope. Note that the X-ray, radio, and optical observations are not contemporaneous.

4. ORIGIN OF X-RAY EMISSION

4.1. Distribution of intrinsic absorption

Figure 1 shows a histogram of the intrinsic absorption associated with the dominant component (in terms of unabsorbed 1-keV flux density) of X-ray emission in each of the sources. Note that some *sources* have two *components* of X-ray emission. 3C 388 is not included on this plot, as the detection of its nucleus is somewhat uncertain, and its intrinsic absorption is unconstrained (see Appendix A). The distribution of core intrinsic absorption is essentially bimodal, with 9 sources having no intrinsic absorption detected and 7 having absorption in excess of 10^{23} atoms cm^{-2}. One might expect absorbing columns of $N_{\rm H} \gtrsim 10^{23}$ atoms cm^{-2} when X-ray emission is surrounded by a dense, dusty structure, such as the putative torus (e.g., Urry & Padovani 1995).

From Figure 1, it is clear that X-ray emission components in FRI-type radio galaxies tend to have much lower intrinsic absorption than FRII-type radio galaxies. This may suggest an intrinsic difference in the nuclear emission characteristics of FRI- and FRII-type sources, a subject that we shall return to in Section 6. Note that the FRII-type radio galaxy 3C 390.3 is cross-hatched in Figure 1. This is because it is a broad-line source, which means that, in the unified scheme of AGN, it is likely to be oriented to the observer such that the inner regions of its AGN are exposed, unlike the other FRII-type sources.

4.2. The radio core – X-ray core correlation

Figure 2a shows a plot of the unabsorbed 1-keV X-ray luminosity density against the 5-GHz VLA unresolved radio core luminosity density of each X-ray component of emission of all the sources presented in Table 4, while Figure 2b shows a plot of the unabsorbed 1-keV and 5-GHz flux densities. The components are separated into those with intrinsic absorption less than 5×10^{22} atoms cm^{-2} (*circles*) and those with intrinsic absorption greater than this value (*triangles*). From Figures 2a and 2b, it is evident that the X-ray emission separates into two distinct "bands": in other words, the unabsorbed X-ray luminosities and fluxes of

components with high intrinsic absorption (greater than 5×10^{22} atoms cm^{-2}) tends to lie significantly above than those components with low intrinsic absorption (less than 5×10^{22} atoms cm^{-2}). For components with $N_{\rm H} < 5 \times 10^{22}$ atoms cm^{-2}, we see no correlation between X-ray luminosity and intrinsic absorption. Most interestingly, the X-ray emission of all FRII-type sources is dominated by components of high intrinsic absorption, a subject we shall return to in Section 6.

Figure 1 shows that the majority of X-ray components below the arbitrary 5×10^{22} atoms cm^{-2} cutoff we have adopted have essentially no intrinsic absorption. The highest intrinsic absorption below the cutoff is $\sim 4 \times 10^{22}$ atoms cm^{-2}, which is associated with the second power law in Centaurus A, a galaxy noted for its strong and complex dust lane. The next two highest intrinsic absorptions measured below the cutoff are in 3C 83.1B and 3C 296, two galaxies observed to possess highly inclined dusty disks (Chiaberge et al. 1999). In Section 4.5 we present evidence that the intrinsic absorption associated with these components is due to gas in the host galaxy. The intrinsic absorption of X-ray components above the cutoff ranges from $\sim$1–6$\times10^{23}$ atoms cm^{-2} and is unlikely to be due to gas in the host galaxy, and is more plausibly associated with denser gas and dust close to the nuclei, such as a dusty torus.

In Figures 2a and 2b, we identify the broad-line FRII-type radio galaxy 3C 390.3 which is likely to be oriented to the observer such that the inner regions of the AGN are exposed. We also identify 3C 388, the only low-excitation FRII-type radio galaxy in the sample. As discussed in Appendix A, its spectrum is uncertain, and may be modeled with either no intrinsic absorption, or an intrinsic absorption of $\sim10^{23}$ atoms cm^{-2}, consistent with that of the other FRII-type radio galaxies we analyzed. We therefore include *two* data points for 3C 388, to illustrate this. Finally, we note that the X-ray spectrum of 3C 321 is somewhat uncertain, meaning that no tight constraints can be placed on the strength of its heavily absorbed emission, while the poor signal-to-noise spectrum of 3C 449 means that it is only possible to place an upper limit on its continuum emission.

In summary, the observed separation of those components with low and high intrinsic absorption may suggest that different physical emission processes are responsible for each. In what follows, we investigate this hypothesis further.

4.3. Components with low intrinsic absorption: A jet origin

In this section, we consider those components of X-ray emission with low intrinsic absorption ($N_{\rm H} < 5 \times 10^{22}$ atoms cm^{-2}), excluding the broad-line radio galaxy 3C 390.3. The

mean photon index for these components is 1.88 ± 0.02. A strong correlation is apparent, in both the X-ray/radio luminosity-luminosity and flux-flux plots (Figure 2). Analysis with the astronomical survival analysis package (ASURV — Lavalley et al. 1992) implementation of the modified Kendall τ algorithm, taking into account the censoring of the X-ray data, shows that the luminosity-luminosity and flux-flux correlations are significant at the 99.8% and 99.95% significance levels, respectively. That the correlation in the flux-flux relationship is significant gives confidence that we are not simply seeing an artificial redshift-induced artifact in the luminosity-luminosity relationship. Some scatter still exists in the distribution, although this may simply be due to variability and the non-contemporaneous nature of the X-ray and radio data (see, e.g., Evans et al. 2004 and Evans et al. 2005 for discussions related to Cen A and NGC 6251).

In order to provide a quantitative analysis, we determined the slope of the core flux-flux and luminosity-luminosity plots using linear regression. Performing linear regression of this dataset is hampered by the fact that some of the data points are upper limits, rather than detections, and so we use the Buckley-James method of linear regression, as implemented in ASURV, which takes into account censored data. We calculated the best-fit slope by taking the bisector of the two lines of best fit obtained by the Buckley-James regression of each variable (i.e., the radio and X-ray flux/luminosity) on each other. Taking the bisector is important so that one quantity is not privileged over the other by being treated as the independent variable in the analysis (see discussion by Hardcastle & Worrall 1999). For the luminosity-luminosity plot, we find the best-fitting slope to be 0.91 ± 0.17, and for the corresponding flux-flux plot, we find the best-fitting slope to be 1.06 ± 0.16.

The observed correlation implies a physical relationship between the X-ray emission and jet-generated radio-core emission of sources with components of low intrinsic absorption. This confirms previous work (e.g., Worrall & Birkinshaw 1994; Hardcastle & Worrall 1999; Canosa et al. 1999) that found a correlation between the soft X-ray emission measured with *ROSAT* and the radio core emission of radio galaxies. It is therefore plausible that the X-ray emission has an origin at the base of the radio jet, on scales larger than any torus. This is not the only interpretation; for example, Donato et al. (2004) suggest that the soft X-ray emission may have an origin in an accretion flow and that an obscuring torus is *absent*.

VLBI observations of parsec-scale radio jets (e.g., Pearson 1996; Giovannini et al. 2001) show evidence for relativistic bulk motion, often with Lorentz factors in excess of 5, which implies that the radio cores observed with the VLA are likely to be affected by beaming. Indeed, although the intrinsic radio powers of these sources are similar, the distribution of core prominences (defined as the ratio of 5-GHz VLA core to 178-MHz total flux densities) spans over four orders of magnitude. Hardcastle & Worrall (2000) demonstrated that the

expected distribution of core prominences of a randomly orientated population of radio jets with a single intrinsic core prominence and bulk Lorentz factor 5 replicates the distribution of observed core prominences, and is consistent with the hypothesis that the unresolved VLA cores are strongly affected by relativistic beaming. Therefore, the existence of the radio–X-ray flux and luminosity correlations suggests that the X-ray emission is also affected by beaming. The simplest mechanism for this is that the X-ray and radio emission have a common origin in the relativistic electron population in a jet. If the X-ray emission of components of low intrinsic absorption were instead associated with the accretion flow, then the observed correlations between the radio and X-ray fluxes and luminosities would not necessarily be expected. Indeed, although Merloni et al. (2003) found a positive correlation between the X-ray and radio luminosities in a sample of both radio-quiet (but not silent) and radio-loud sources, the scatter is as much as 5 orders of magnitude. In our present sample, which selects only radio-loud sources, the scatter in X-ray components likely to have a jet origin is significantly less than the radio-quiet sources in the Merloni et al. (2003) sample, whose X-ray emission is dominated by an accretion flow.

We note that there is no distinction between these components of X-ray emission associated with FRI- and FRII-type radio galaxies: each of the FRII sources, although being dominated by heavily obscured emission, has a component of X-ray emission with low intrinsic absorption that lies on the same trendline as the FRI components. In Figure 3, we show a plot of the 1-keV luminosity density against the 5-GHz radio luminosity density for the FRI- and FRII-type sources, which illustrates this point.

The observed range in photon indices is consistent with either a synchrotron or inverse-Compton mechanism for the jet-related X-ray emission. The dispersion in the photon indices could be explained by a two-component synchrotron+SSC model in which varying the beaming parameter causes one component to dominate over the other.

4.4. Components with high intrinsic absorption: An accretion origin

In this section, we consider those X-ray components with intrinsic absorption greater than 5×10^{22} atoms cm^{-2}. The mean photon index of these components is 1.76 ± 0.02 and is significantly flatter than that of components with low intrinsic absorption ($\Gamma = 1.88 \pm 0.02$). The observed range of photon indices in these components of X-ray emission is consistent with that measured in a sample of ASCA observations of broad-line radio galaxies (Sambruna et al. 1999). It is evident from Figures 2a and 2b that the unabsorbed X-ray luminosity and flux densities of these components lie approximately 2 orders of magnitude above those components with intrinsic absorption less than 5×10^{22} atoms cm^{-2}. Intrinsic absorption in

excess of 10^{23} atoms cm^{-2} is unlikely to be simply due to dust in the host galaxy, as this would imply that very strong ($A_{\rm V} = 50$) dust lanes and/or molecular clouds would have to be placed fortuitously in each of these objects to obscure the nucleus. Instead, we argue that the absorption is consistent with an origin in a dusty structure surrounding the nucleus, such as the putative torus. From Figure 2b we note that the correlation between the radio and X-ray flux densities of these components appears weaker than those with $N_{\rm H} < 5 \times 10^{22}$ atoms cm^{-2} that were interpreted to have a physical origin in the form of a beamed radio jet. Indeed, analysis with the Kendall τ-test shows that the significance of this correlation is 91.7%. However, it is only by sampling a larger number of FRII-type sources that we can determine if this correlation is in fact weaker.

While the chosen cutoff of 5×10^{22} atoms cm^{-2} was in a sense arbitrary, an obvious physical difference in the emission processes of the two "bands" of X-ray emission manifests itself: those sources dominated by a component of emission with high intrinsic absorption all have fluorescent Kα line-emission from neutral or near-neutral states of iron, whereas those with low intrinsic absorption do not. The line parameters are consistent with an origin in cold material, either from the outer regions of an accretion disk, or from a region still further out, possibly in the form of a torus-like structure that surrounds the nuclear emission.

In summary, for components with high intrinsic absorption ($N_{\rm H} > 10^{23}$ atoms cm^{-2}), we have shown that:

1. Their unabsorbed X-ray flux and luminosity densities lie above those that are likely to have an origin in the form of a jet

2. All are associated with Fe Kα lines

The most probable interpretation for the X-ray emission of these components, therefore, is that they are dominated by an accretion flow and are surrounded by a dusty circumnuclear structure, plausibly in the form of a torus. All narrow-line FRII-type sources show these features. This distinguishes them from FRI-type sources, whose X-radiation is dominated by unabsorbed emission, likely to be related to the jet (with the exception of Cen A). The one exception to the observed properties of components with $N_{\rm H} > 5 \times 10^{22}$ atoms cm^{-2} is 3C 388. Under the assumption that its nuclear emission is obscured by a column of 10^{23} atoms cm^{-2}, its unabsorbed X-ray flux and luminosity densities lie below those of the other sources discussed here. However, 3C 388 is the only low-excitation FRII-type radio galaxy in the sample which, as postulated by Hardcastle (2004), may imply that it is an intrinsically low-jet-power (i.e., more FRI-like) source, with its high 178-MHz radio luminosity due to a

rich surrounding environment (c.f., Barthel & Arnaud 1996). Our measurement of a relatively low X-ray core luminosity for this source is consistent with this argument.

The broad-line radio galaxy 3C 390.3 also shows the same X-ray emission properties as those sources with high intrinsic absorption, in that its X-ray flux and luminosity densities also lie above those sources with low intrinsic absorption. The detection of broad optical emission lines in this source implies, in the context of unified AGN schemes, that it is oriented to the observer such that its accretion system is viewed directly, leading to its high luminosity but low intrinsic absorption. Other pieces of physical evidence support this interpretation, such as the detection of rapid variability and Fe Kα line-emission (Inda et al. 1994; Leighly et al. 1997; Gliozzi et al. 2003), although the fluorescent iron line is only detected marginally in our limited signal-to-noise *Chandra* observation.

In order to consider the possible structure of the accretion flow in the components with high intrinsic $N_{\rm H}$, we compared their X-ray and Eddington luminosities. Out of these high-$N_{\rm H}$ sources, it is only for Centaurus A (Marconi et al. 2001) and Cygnus A (Tadhunter et al. 2003) that estimates of the black hole mass from dynamical motions of stellar kinematics are available. The black hole masses of the other sources, where available, are taken from Bettoni et al. (2003) and Marchesini et al. (2004), who assume that they lie on the previously established correlation between the mass of the black hole and the host bulge magnitude (e.g., Ferrarese & Merritt 2000). As there exists considerable scatter in this relation, these black hole estimates are somewhat uncertain. Taking the black hole masses at face value, we tabulate, for each source, its 0.5–10 keV unabsorbed X-ray luminosity, Eddington luminosity, and the ratio of these two quantities ($\eta_{\rm X,Edd}$). The results are shown in Table 5.

Under the assumption that the sources accrete at the Eddington limit, from Table 5, it can be seen that $\eta_{\rm X,Edd}$ for these sources typically ranges from $\sim 10^{-3}$ to $\sim 10^{-2}$, with the value for Cen A somewhat lower at $\sim 10^{-5}$. However, it should be noted that the efficiency is based only on the 0.5–10 keV X-ray luminosity of the source, *not* its bolometric luminosity, which could typically be a factor of 3 to 10 times higher (Elvis et al. 1994). Indeed, for Cygnus A (3C 405), Tadhunter et al. (1993) estimate a bolometric luminosity of between 5×10^{45} and 2×10^{46} ergs s^{-1}, placing its efficiency at $\sim 5 \times 10^{-2}$.

Although the efficiency values are uncertain, it seems that the accretion flows in these sources tend to have relatively high $\eta_{\rm X,Edd}$, which would suggest a significant contribution to the emission from a standard, geometrically thin, optically thick accretion disk (e.g., Shakura & Sunyaev 1973), rather than a radiatively inefficient ADAF-type accretion flow (e.g., Narayan & Yi 1995). The efficiency of Cen A is lower than those of the other components studied here, which may imply that its accretion flow takes the hybrid form of a radiatively inefficient optically thin inner component surrounded by a standard thin disk,

as discussed more fully by Evans et al. (2005).

4.5. Optical constraints

In Figure 4 we plot the unresolved red optical luminosity densities (mostly measured using the F702W filter of the *HST*'s WFPC2 instrument) and 1-keV X-ray luminosity densities of the components of emission associated with each source, where *HST* data exist. As in Section 4.2, we separate the X-ray components into those with intrinsic absorption less than and greater than 5×10^{22} atoms cm^{-2}. Again, it can be seen that a good correlation exists between the optical and X-ray luminosities and fluxes of those components with intrinsic absorption less than 5×10^{22} atoms cm^{-2}, as found previously by, e.g., Hardcastle & Worrall (2000). In a similar manner to the radio and X-ray plots, components with intrinsic absorption greater than 5×10^{22} atoms cm^{-2}, together with 3C 390.3, produce more X-ray emission than those with intrinsic absorption below this value.

The *HST* data allow a test of the postulate that the intrinsic absorption of components with $N_{\rm H} < 5 \times 10^{22}$ atoms cm^{-2} is associated with dust in the host galaxy. *HST* observations of low-redshift FRI-type radio galaxies in the 3C catalogue (Chiaberge et al. 1999) reveal a variety of structures, including dust lanes and a series of dusty disks oriented at a large range of angles to the observer. Aside from Centaurus A, the two sources with the highest intrinsic absorption below the imposed 5×10^{22} atoms cm^{-2} cutoff, 3C 83.1B and 3C 296, are associated with host galaxies with circumnuclear disks at high inclinations to the observer. Figure 4 shows that these two sources also have the highest deficit of optical emission with respect to X-ray emission, which indeed suggests that they are most affected by absorption.

5. CONSTRAINTS ON A TORUS IN FRI-TYPE RADIO GALAXIES

If, as seems likely, the X-ray emission of the nuclei of FRI-type galaxies is dominated by the base of a relativistic jet that occurs on scales larger than that of any putative torus, one cannot determine directly the presence or absence of the torus, weakening the claim by Donato et al. (2004) that the torus is absent in these sources. However, inferences can be made about its presence, and in this section, we test the hypothesis that a torus is present in FRI-type nuclei.

Let us assume that, in addition to the dominant jet component of X-ray emission, there exists a 'hidden' component of accretion-related emission of photon index 1.7 obscured by a torus of intrinsic absorption 10^{23} atoms cm^{-2}. This choice of obscuration and photon index

is consistent with that measured in Centaurus A and the heavily absorbed FRII-type radio galaxies discussed in Section 4.4, and the photon index is close to the value measured for a sample of type 2 Seyfert galaxies observed with *ASCA* (Turner et al. 1997). For each 'hidden' component, we then consider the 90%-confidence upper limits to its 0.5–10 keV luminosity. As an example, consider 3C 264. Its nuclear spectrum is modeled by a single, unabsorbed power law. Adding a component of heavily absorbed emission to the model fit, refitting the spectra, and determining the 90%-confidence errors, yields an upper limit to the 0.5–10 keV luminosity of 3.3×10^{40} ergs s^{-1} for this component. In Table 6, we repeat this exercise for all FRI-type nuclei with low intrinsic absorption ($N_{\rm H} < 5 \times 10^{22}$ atoms cm^{-2}), and also show the black hole mass, Eddington luminosity, and upper limits on $\eta_{\rm X,Edd}$ of each source. The black hole masses quoted are taken from the black hole mass–host galaxy magnitude correlation described in Section 4.4, although kinematic mass estimates are available for 3C 272.1 (M84) (Bower et al. 1998), 3C 274 (M87) (Ford et al. 1994), and NGC 6251 (Ferrarese & Ford 1999).

None of the values of the primary (detected) power-law photon index of the unobscured component varies significantly with the addition of this hidden component. We find that, under the assumption of obscuration by a column of 10^{23} atoms cm^{-2}, the upper limits to any hidden, accretion-related luminosities are all in the range 10^{39}–10^{41} ergs s^{-1}. The highest hidden luminosities cannot exceed that of the heavily absorbed (and likely accretion-related) component measured in the FRI-type radio galaxy Centaurus A ($\sim 5 \times 10^{41}$ ergs s^{-1}), but some have maximum possible luminosities that are one to two orders of magnitude lower than this. In addition, *all* have upper limits to the 0.5–10 keV luminosities and Eddington efficiencies several orders of magnitude less than those of the accretion-related components in the FRII sources, whose mean luminosity is $\sim 4 \times 10^{43}$ ergs s^{-1}. (Again, we note that the low-excitation FRII-type radio galaxy 3C 388 is an exception here).

A similar calculation for an absorbing column of 10^{24} atoms cm^{-2} (Table 6) still does not permit FRI-type sources to possess hidden accretion components with efficiencies $\eta_{\rm X,Edd}$ comparable with those of the FRII-type sources. This suggests that the accretion flows of FRI-type sources radiate at lower efficiency than do FRII-type sources, and may for example take the form of optically thin ADAFs (e.g., Narayan & Yi 1995; Esin et al. 1997).

6. A NUCLEAR FANAROFF-RILEY DICHOTOMY?

We have considered the correlations between the flux and luminosity densities of the X-ray, radio, and optical components of nuclear emission and argued that the X-ray emission of FRI-type radio-galaxy nuclei is most likely dominated by emission from a parsec-scale jet, with little or no intrinsic absorption. By contrast, the emission of FRII-type radio-

galaxy nuclei is dominated by an accretion flow and is heavily absorbed (with the exception of the broad-line radio galaxy 3C 390.3) and therefore must be surrounded by a dusty structure, such as the putative torus. In addition, each heavily absorbed component has an accompanying component of X-ray emission of intrinsic absorption less than 5×10^{22} atoms cm^{-2}, the detections or upper limits to the flux and luminosity densities of which all lie in the region occupied by those sources likely to have a jet-related origin (see Figure 3).

Our results imply that, for the FRII-type radio galaxies at least, both jet- and accretion-related components of X-ray emission are present, which is consistent with unified models of AGN. Further, we have shown that the data do not exclude the presence of heavily obscured, accretion-related emission in FRI-type radio galaxies, but that it is of lower luminosity than in FRII-type radio galaxies if there is a similar level of obscuration.

It is clear that there tends to be a dichotomy in the observed properties of the X-ray nuclei of FRI- and FRII-type radio galaxies. But why should this dichotomy occur? Is it due to intrinsic differences in the properties of FRI and FRII radio galaxies, or simply due to the relative contributions of jet- and accretion-related emission varying with the total power of the source? In what follows, we discuss alternative models to explain the observed differences in the X-ray emission characteristics of FRI- and FRII-type sources.

6.1. Model 1: FRI-type galaxies have tori of higher intrinsic absorption than FRII-type radio galaxies

In this model, a luminous accretion flow in an FRI-type radio galaxy (of luminosity consistent with those measured in the FRII-type radio galaxies) is surrounded by a torus of higher intrinsic absorption than the FRII-type radio galaxies. Such a model gives rise to a reduced contribution from the accretion system in terms of observed X-ray flux, such that the jet dominates the X-ray emission. In Table 6, we showed that even if a Compton-thick ($N_{\rm H} \sim 10^{24}$ atoms cm^{-2}) torus were to obscure the accretion-related emission of jet-dominated FRI-type sources, the luminosities and efficiencies are still somewhat lower than those of the FRII-type sources (see Table 5). Thus it seems that if a torus obscures FRI-type accretion flows, the luminosities of FRII-type accretion flows are still higher, unless the intrinsic absorption of the torus in FRI-type sources is extreme ($N_{\rm H} > 10^{24}$ atoms cm^{-2}).

Evidence against this model comes from constraints from infrared data. If FRI-type radio galaxies do indeed harbor luminous accretion flows surrounded by very dusty structures, one would expect to detect significant infrared emission in the centers of these sources. Such a scenario may be ruled out from *ISO* observations of a sample of 3CR FRI- and FRII-type

radio galaxies (Müller et al. 2004; Haas et al. 2004). None of the FRI sources exhibits any high MIR or FIR dust luminosity, which would be expected for an intrinsically powerful, but highly obscured AGN (c.f., the FRII sources, in which strong MIR and FIR emission is observed).

Based on the above arguments, it seems unlikely that the accretion flows of FRI-type sources are obscured by tori of higher intrinsic absorption than in FRII-type sources. This then implies that FRI-type accretion flows are less luminous than their FRII-type counterparts, either due to a lower radiative efficiency or lower accretion rate. In the immediate future, *Spitzer* observations of all 36 3CRR sources at $z < 0.1$ (Birkinshaw et al., in prep.) will test this hypothesis further.

6.2. Model 2: The relative contribution of accretion-related and jet-related emission varies smoothly as a function of total AGN power

In this model, the fraction of jet- and accretion-related emission varies with AGN power in such a way that, at higher AGN powers, accretion-related emission comes to dominate over jet-related emission. In this scenario, an intrinsic dichotomy between the properties of FRI- and FRII-type radio-galaxy nuclei need not exist, and the observed properties would simply be due to a smooth scaling relation with AGN power. The 178-MHz luminosity density of a source is an approximate measure of its AGN power since (1) it correlates reasonably well with jet power (Fanaroff & Riley 1974) and (2) jet power correlates reasonably well with the narrow-line luminosity of AGN (Rawlings & Saunders 1991).

In order to test this model, in Figure 5 we plot the 1-keV X-ray accretion-flow luminosity density (either modeled from the spectra in the case of the FRII-type sources and Cen A, or upper limits in the case of the FRI-type sources) against the 178-MHz luminosity density. Although there is considerable scatter, it is plausible that there exists an underlying correlation between the 178-MHz luminosity densities and 1-keV luminosity densities of the accretion-related components, which may support this model.

This model can explain the observed differences in the X-ray emission characteristics of FRI- and FRII-type sources *without* having to invoke an intrinsic dichotomy in the nuclear properties of the two populations. Nevertheless, this model leaves unexplained the fact that the transition between the X-ray emission of a source being jet-dominated and accretion-dominated should occur so close to the FRI/FRII boundary, rather than there being a significant population of jet-dominated FRII-type sources or, conversely, accretion-dominated FRI-type sources. However, a possible resolution to this problem is in the model proposed

by Falcke et al. (1995), in which the opening angle of the torus is proportional to the power of the accretion flow. At low accretion-flow power, the opening angle of the torus is such that material from it becomes stripped and entrained into the jet flow, eventually causing the observed deceleration of the jet on kiloparsec scales, leading to an FRI-type large-scale morphology. As soon as the torus opening angle becomes greater than the opening angle of the jet, the entrainment is not as severe, allowing the jet to remain highly relativistic and produce an FRII-type source.

Another potential problem with this model is that at the FRI/FRII boundary of $\sim 10^{25}$ W Hz^{-1} sr^{-1}, the accretion-related luminosity of the FRII-type source 3C 98 is 1.5 orders of magnitude greater than the upper limits on that in the jet-dominated FRI-type sources 3C 338 and 3C 465. In other words, it is impossible to 'hide' an accretion flow of the luminosity of 3C 98 in these two jet-dominated sources of comparable 178-MHz power, unless the intrinsic absorption is extreme. This may at first suggest that the luminosity of the accretion-related emission does *not* scale smoothly with the 178-MHz luminosity density. However, we note that the model of Falcke et al. (1995) may provide an adequate explanation of the above effect, and that only these 3 of the 8 3CRR sources that span the boundary have been observed with *Chandra* or *XMM-Newton*. It is important to test this model by observing the remaining 5 3CRR sources.

6.3. Model 3: An intrinsic dichotomy exists in the accretion-flow structures of FRI- and FRII-type sources

It has previously been proposed (e.g., Reynolds et al. 1996; Donato et al. 2004) that there exists a fundamentally different accretion *mode* in FRI- and FRII-type sources, such that the accretion-flow luminosities and radiative efficiencies of FRI-type radio galaxies are systematically lower than those of FRII-type radio galaxies, consistent with our observations.

The most widely discussed interpretation in this context is one in which the fractional mass accretion rate $\dot{m} = \dot{M}/M$ governs the contribution to the emission from a radiatively inefficient optically thin advection-dominated accretion flow (ADAF). Esin et al. (1997) argued for black-hole X-ray binaries that there exists a critical fractional mass accretion rate $\dot{m}_{\rm crit}$ below which gas is unable to cool efficiently, such that the accretion-flow energy is advected into the black hole, forming an ADAF. Above $\dot{m}_{\rm crit}$, the accretion flow makes the transition to being dominated by a standard, radiatively efficient, geometrically thin, optically thick disk (e.g., Shakura & Sunyaev 1973), with a step increase in the total accretion-flow luminosity. By analogy, in radio galaxies, the accretion flow of FRI-type radio galaxies may take the form of a radiatively inefficient ADAF-type model, whereas in FRII-type galaxies it is

more likely to form a Shakura-Sunyaev disk.

This model resolves the two main issues of Model 2. Firstly, it no longer requires there to be a coincidence that the transition from a source being jet-dominated to accretion-dominated occurs at the FRI/FRII divide, since this is a consequence of the different accretion-flow modes in FRI- and FRII-type sources. Secondly, it explains why the luminosity of the accretion flow of 3C 98 is significantly higher than those of the two jet-dominated FRI-type sources that lie at comparable 178-MHz luminosity: the accretion-flow luminosity of 3C 98 has a significant contribution from a Shakura-Sunyaev accretion disk, whereas those of 3C 338 and 3C 465 are likely to be dominated by a radiatively inefficient, optically thin accretion flow. Again, however, it is important to test this model by observing the remaining sources that populate the FRI/FRII break in 178-MHz radio luminosity.

The major uncertainty is how a dichotomy in the subparsec-scale accretion-flow mode could influence the deceleration of jets into FRI- and FRII-type structures, which is observed to occur on kiloparsec scales (e.g., Bicknell 1995; Gopal-Krishna & Wiita 2000; Müller et al. 2004). For this model to remain viable, we speculate that, although differing accretion-flow modes may exist, the jet-production mechanism must be the same in the nuclei of FRI- and FRII-type sources.

One notable exception to the above models is the nuclear emission of Centaurus A. As the only FRI-type radio galaxy whose X-ray emission is heavily obscured and dominated by an accretion flow, its nuclear X-ray emission is more similar to that of the FRII-type sources. One possible resolution of this problem is that the recent merger that has occurred in Cen A may have provided additional material to accrete onto the supermassive black hole, triggering heightened nuclear activity and a new phase of radio activity, causing the supersonic re-inflation of the lobes (Kraft et al. 2003).

7. CONCLUSIONS

We have presented results from a *Chandra* and *XMM-Newton* spectral analysis of the nuclei of a sample of the nuclei of 22 low-redshift ($z < 0.1$) radio galaxies. We find that:

1. The nuclear X-ray spectra of FRI-type sources are unabsorbed, or absorbed simply by gas related to the known kpc-scale dusty disks in the host galaxy. The strong observed correlations between the X-ray, radio, and optical fluxes and luminosities imply that the emission has a common origin at the base of a relativistically beamed parsec-scale jet.

2. The nuclear X-ray emission of narrow-line FRII-type sources is dominated by heavily absorbed components of emission with $N_{\rm H} > 10^{23}$ atoms cm^{-2}, and is accompanied by emission from neutral fluorescent Fe Kα lines. We argue that this absorbed emission is likely to originate in an accretion flow and be surrounded by a structure such as the putative torus. We also find that the nuclear X-ray spectrum of every FRII galaxy has a corresponding component of soft X-ray emission, which is consistent with having a jet-related origin.

3. If the (jet-dominated) X-ray emission of FRI-type sources occurs on scales larger than the torus, it is impossible to test for the presence of a torus using the X-ray data, but important constraints can still be made. We estimate the maximum level of a 'hidden', accretion-related component of emission that could be obscured by an adopted column of 10^{23} atoms cm^{-2} to be in the range 10^{39}–10^{41} ergs s^{-1}. The X-ray data do not exclude the presence of a torus, but the luminosity of the accretion flow it obscures is significantly less than in FRII-type sources unless there is more obscuring matter in the FRI-type sources, which seems unlikely based on infrared constraints.

4. Any 'hidden' accretion flows in jet-dominated FRI-type sources are likely to be significantly sub-Eddington in nature. This implies that their accretion flows are mass-starved, and/or radiate at a low efficiency.

5. The accretion-flow luminosities of FRII-type sources are typically several orders of magnitude higher than those of FRI-type sources. The ratio of X-ray to Eddington luminosities, $\eta_{\rm X,Edd}$, is $\sim 10^{-3}$–10^{-2}, while the ratio of bolometric to Eddington luminosities is still higher. This implies that the accretion flows of FRII-type sources tend to be fed at a high rate, and/or possess significant contributions from high-radiative-efficiency flows, plausibly in the form of a standard, geometrically thin, optically thick disk.

6. Two models may account for the observed differences in the nuclear properties of FRI- and FRII-type sources, although neither is without problems. One model, in which the relative contribution of the accretion-related and jet-related emission varies smoothly as a function of total AGN power, can successfully account for the observed X-ray emission characteristics of these sources. However, it is then difficult to understand why the transition between a source being jet-dominated and accretion-dominated occurs at the FRI/FRII boundary. Alternatively, there is a real dichotomy in the accretion-flow modes of FRI- and FRII-type sources. We note that the manner in which the accretion-flow mode might then affect the large-scale (FRI versus FRII) characteristics of radio galaxies remains poorly understood.

We are grateful for support for this work from PPARC (a Studentship for D.A.E. and research grant for D.M.W.), the Royal Society (Research Fellowship for M.J.H.), and NASA (contracts NAS8-38248 and NAS8-39073 with the Smithsonian Astrophysical Observatory). We thank Oliver Shorttle for providing the results from his *HST* analyses of these sources, and Elena Belsole for useful discussions. We are grateful to the anonymous referee for useful comments.

A. NOTES ON INDIVIDUAL SOURCES

A.1. 3C 31

We initially attempted to model the source spectrum with a single, unabsorbed, power law. However, the fit was poor ($\chi^2 = 49.3$ for 27 dof), with strong residuals at $\sim$1 keV, suggesting that a contribution from thermal emission is necessary. The fit was substantially improved ($\Delta\chi^2 = 39.7$ for two additional parameters) by adding a thermal (APEC) model of temperature $kT = 0.68^{+0.08}_{-0.07}$ keV, abundance 0.3 of solar, and normalization $(3.39^{+0.80}_{-0.85})\times10^{-5}$. No further significant improvement was obtained by including intrinsic absorption in the model fit. The 1-keV flux density and spectral index are consistent with previously published *Chandra* results (Hardcastle et al. 2002; Donato et al. 2004). The 0.5–5 keV radial surface-brightness shows a deficit of counts approaching a factor of 2 compared with those measured spectrally. As discussed by Hardcastle et al. (2002), the discrepancy may be resolved by postulating that there exists an additional, unresolved dense component of thermal emission that lies close to the core.

A.2. 3C 33

A variety of simple models were fitted to the nuclear spectrum but all yielded poor results. The first acceptable fit ($\chi^2 = 49.0$ for 39 dof) was obtained with a model consisting of a heavily absorbed power law [$N_{\rm H} = (3.9^{+0.7}_{-0.6})\times10^{23}$ atoms cm^{-2}], a $\sim$6.4 keV Gaussian Fe Kα emission line of equivalent width 320^{+340}_{-160} eV, and a second, unabsorbed power law. When adding intrinsic absorption to the second power-law component, the best fitting column density tended to 0. No significant improvement in the fit ($\Delta\chi^2 = 8.21$ for three additional parameters) was obtained by adding a component of thermal emission (the probability of achieving a larger F by chance is 8.2%). The photon indices of both power laws were fixed at 1.7, owing to the large number of free parameters already present in the model. The 1-keV flux densities are largely insensitive to this choice, however.

A.3. 3C 66B

A model consisting of a single, unabsorbed, power law provided a good fit to the data ($\chi^2 = 40.3$ for 36 dof). The best-fitting power law photon index is $\Gamma = 2.25 \pm 0.11$. Adding thermal emission of temperature $0.41^{+0.23}_{-0.10}$ keV, abundance half of solar, and normalization $(2.67^{+1.76}_{-1.60}) \times 10^{-5}$ to the spectral model significantly improved the fit ($\chi^2 = 29.1$ for 34 dof). In this case the photon index is 2.03 ± 0.18. A model consisting of an absorbed power law and thermal emission failed to improve the fit ($\Delta\chi^2 = 2.7$ for 1 additional parameter, with a probability of achieving a greater F by chance of 7.6%). We compared the results of our spectral analysis with previously published work (Hardcastle et al. 2001; Donato et al. 2004), and found the 1-keV power-law flux density to be consistent.

A.4. 3C 83.1B (NGC 1265)

We attempted to fit several models to the nuclear spectrum of 3C 83.1B, but found that the only one that gave an acceptable fit ($\chi^2 = 9.45$ for 12 dof) consisted of the sum of an absorbed power law and thermal emission of abundance 0.3 of solar. The best fitting spectral parameters for this model are $N_{\rm H} = (3.2^{+0.8}_{-0.7}) \times 10^{22}$ atoms cm^{-2}, $\Gamma = 2.00^{+0.27}_{-0.20}$. The temperature of the thermal component is $0.58^{+0.15}_{-0.14}$ keV, with normalization $(9.69^{+2.95}_{-2.74}) \times 10^{-6}$. These parameters are consistent with those measured by Sun et al. (2005), who performed the original observation.

A.5. 3C 84 (NGC 1275)

A model fit consisting of power law plus a single thermal component failed to provide an adequate fit to the spectrum ($\chi^2 = 1322.8$ for 1155 dof). An acceptable fit ($\chi^2 = 1165.3$ for 1153 dof) was achieved with the combination of a power law and *two* thermal components, one of temperature 0.77±0.04 keV, solar abundance, and normalization $(8.33^{+1.00}_{-1.33}) \times 10^{-4}$; the other of temperature 2.74±0.10 keV, abundance half of solar, and normalization $(9.72^{+0.50}_{-0.72}) \times 10^{-3}$. However, a third thermal component, fitted by Donato et al. (2004), is not found here. Instead, an additional significant improvement in the fit ($\Delta\chi^2 = 9.35$ for two additional parameters) was achieved by the addition of a Gaussian emission line with a centroid energy $6.39^{+0.08}_{-0.09}$ keV and frozen (unresolved) linewidth of 10 eV and equivalent width 26^{+46}_{-22} eV. We compared our results with previously published work (Donato et al. 2004), and find the 0.3–8 keV unabsorbed luminosity of the power law to be approximately consistent.

A.6. 3C 98

A model fit consisting of a heavily absorbed power law [$N_{\rm H} = (1.1 \pm 0.2) \times 10^{23}$ atoms cm^{-2}; $\Gamma = 1.56 \pm 0.26$] and thermal emission [$kT = 0.98 \pm 0.12$ keV] provided a good fit to the data ($\chi^2 = 40.7$ for 42 dof). However, an adequate fit ($\chi^2 = 47.1$ for 42 dof) was also achieved with the sum of two power laws, one heavily absorbed [$N_{\rm H} = (1.5 \pm 0.2) \times 10^{23}$ atoms cm^{-2}; $\Gamma = 1.87 \pm 0.32$], and the other with no absorption and a frozen photon index of 2. Both fits were improved when an unresolved Gaussian Fe Kα line of linewidth frozen at 10 eV was added; the improvements in the fits were $\Delta\chi^2 = 8.0$ and $\Delta\chi^2 = 7.4$, respectively, for two additional parameters. A model consisting of a heavily absorbed power law, an unabsorbed soft power law, a Gaussian Fe Kα line and thermal emission, did not significantly improve the fit over the previous two models ($\chi^2 = 30.7$ for 39 dof).

ROSAT observations of 3C 98 (Hardcastle & Worrall 1999) show extended X-ray emission on scales of tens of arcseconds, in addition to an unresolved core. It is therefore likely that the most appropriate spectral model for this source is the one consisting of a heavily absorbed power law [$N_{\rm H} = (1.2^{0.3}_{-0.2}) \times 10^{23}$; $\Gamma = 1.68^{+0.23}_{-0.37}$], a Gaussian Fe K$\alpha$ [$E = 6.37 \pm 0.10$ keV; equivalent width 240^{+250}_{-170} eV], and thermal emission [$kT = 0.98 \pm 0.12$ keV; abundance 0.3 of solar; normalization $(6.21 \pm 1.33) \times 10^{-5}$]. We note that the upper limit on the flux density of the statistically insignificant unabsorbed power law (which might be regarded as jet-related nuclear emission) is an interesting quantity. We compared the results of our *XMM-Newton* spectral fitting with previously published work (Isobe et al. 2005). These authors measure a 2–10 keV unabsorbed luminosity of $(4.6^{+0.7}_{-0.6}) \times 10^{42}$ ergs s^{-1}, consistent with the value we measure of $(5.4^{+1.4}_{-2.6}) \times 10^{42}$ ergs s^{-1}. The photon indices and temperature of the thermal emission are also consistent.

A.7. 3C 264

The nuclear spectrum is well modeled by a single, unabsorbed, power law of photon index $2.34^{+0.07}_{-0.08}$. For this fit, we found the value of χ^2 to be 123.0 for 147 dof. No improvement to the fit was achieved with more complex spectral models, such as an intrinsically absorbed power law or the addition of thermal emission: in every case, the values of absorption and thermal normalization tended to zero. We compared the results of our spectral fitting to that from an *XMM-Newton* observation (Donato et al. 2004). The power-law photon indices are approximately consistent ($\Gamma = 2.34^{+0.07}_{-0.08}$ for *Chandra* and $\Gamma = 2.48 \pm 0.04$ for *XMM-Newton*), as are the integrated X-ray luminosities.

A.8. 3C 272.1 (M84)

A single power law provided an acceptable fit to the nuclear spectrum ($\chi^2 = 30.3$ for 25 dof). However, the fit was significantly improved ($\Delta\chi^2 = 19$ for one additional parameter), with the inclusion of relatively mild intrinsic absorption [$N_{\rm H} = (1.9^{+0.9}_{-0.7}) \times 10^{21}$ atoms cm^{-2}] at the redshift of 3C 272.1. No statistically significant improvement in the fit was achieved with the inclusion of a thermal APEC model, which implies that the local background subtraction has accounted for most of the extended thermal emission. We compared the results of our spectral fitting with previously published *Chandra* work (e.g., Harris et al. 2002), and found the power-law photon index, normalization and intrinsic absorption to be consistent. Using the same *Chandra* data, Donato et al. (2004) determined the best-fitting spectral model to be the sum of an absorbed power law and thermal emission. The detection of thermal emission by Donato et al. (2004) is likely due to the selection of an off-source region from which to extract the background spectrum. The intrinsic absorption and photon index we measure agree with the analysis by Donato et al. (2004), and the integrated power-law luminosity is approximately consistent.

A.9. 3C 274 (M87)

A model fit to the spectrum consisting of a single, unabsorbed, power law provided an acceptable fit to the data ($\chi^2 = 97.8$ for 100 dof). However, this fit was significantly improved ($\Delta\chi^2 = 13.6$ for two additional parameters) with the addition of a thermal component, characterized by an APEC model of temperature $0.75^{+0.17}_{-0.14}$ keV, abundance 0.3 of solar, and normalization $(1.11 \pm 0.49) \times 10^{-4}$. Such a temperature in the inner regions of M87 might not be unexpected, as shown from an *XMM-Newton* study of the radially dependent temperatures of the hot, X-ray-emitting gas in this source (Böhringer et al. 2001). The power-law photon index for this fit is 2.09 ± 0.06. For this model, $\chi^2 = 84.2$ for 98 dof, with the probability of achieving a greater F by chance 0.07%. No further statistically significant improvements to the fit were achieved with more complex spectral models. We compared the results of our *Chandra* nuclear spectral analysis with those found by Wilson & Yang (2002). The power-law photon indices and normalizations are consistent, although Wilson & Yang (2002) found evidence for slight additional absorption ($N_{\rm H} = 3.5^{+1.5}_{-1.4} \times 10^{20}$ atoms cm^{-2}) at the redshift of M87.

A.10. 3C 296

Several simple one-component models were fitted to the nuclear spectrum, but we found that the first acceptable fit was achieved with a model consisting of an absorbed [$N_{\rm H} = (1.5 \pm 0.9) \times 10^{22}$ atoms cm^{-2}] power law of photon index $1.77^{+0.60}_{-0.52}$, accompanied by thermal emission [$kT = 0.8^{+0.3}_{-0.5}$ keV; abundance 0.3 of solar; normalization $(1.16^{+0.42}_{-0.45}) \times 10^{-5}$]. The fit was good: $\chi^2 = 9.3$ for 21 dof. However, an acceptable fit was also achieved with the combination of an absorbed power law with $N_{\rm H} = (2.1^{+1.5}_{-1.7}) \times 10^{22}$ atoms cm^{-2} and photon index $\Gamma = 1.9^{+0.8}_{-0.7}$, and a *second* unabsorbed power law with a photon index frozen at 2. A subsequent radial-profile analysis shows that the number of extended counts measured spectrally and spatially agree for the first model, and so we adopt this model. We performed a comparison between our spectral analysis and previously published *Chandra* results (Hardcastle et al. 2005). The measured values of the intrinsic absorption, power law photon index, and 1-keV flux densities are consistent, as are the parameters of the thermal component.

A.11. 3C 321

Single-component models provided poor fits to the spectrum, with noticeable residuals at high and low energies, together with a residual at ∼6 keV suggesting the presence of Fe Kα line-emission. The first moderately acceptable fit ($\chi^2 = 19.2$ for 9 dof) was achieved with an absorbed [$N_{\rm H} = (8.7 \pm 5.7) \times 10^{21}$ atoms cm^{-2}] power law, a Gaussian Fe Kα emission line, and a thermal component of temperature 0.57 ± 0.04 keV. However, positive residuals at energies $\gtrsim$4 keV were noticeable, suggesting the presence of heavily absorbed emission. A model consisting of a heavily absorbed power law of photon index frozen at 1.7, a strong Gaussian Fe Kα line of equivalent width ∼1 keV, a second unabsorbed power law of photon index frozen at 2, and thermal emission of temperature 0.49 ± 0.15 keV and normalization $(1.33^{+0.53}_{-0.34}) \times 10^{-6}$, provided the best fit to the data ($\chi^2 = 9.8$ for 8 dof). Although the photon indices are frozen at their canonical values [owing to the relatively small number of bins (14) and large number of free parameters], the parameter uncertainties are large.

A.12. NGC 6109

Single-component models of either thermal emission or a power law provided an adequate fit to the nuclear spectrum ($\chi^2 = 7.67$ for 8 dof, and $\chi^2 = 7.46$ for 8 dof, respectively). However, a significant improvement in the fit ($\chi^2 = 1.50$ for 6 dof) was achieved with the combination of a power law [$\Gamma = 1.47 \pm 0.47$] and thermal emission [$kT = 0.63^{+0.14}_{-0.17}$ keV,

abundance 0.3 of solar, normalization $(1.01^{+0.41}_{-0.42}) \times 10^{-6}$].

A.13. 3C 338

Simple one-component models of either thermal emission or a power law provided adequate fits to the data ($\chi^2 = 1.66$ and 4.47 for 3 dof, respectively). The best-fitting parameters for the power-law model are $\Gamma = 2.37 \pm 0.81$ with a 1-keV normalization $(5.2^{+2.1}_{-2.1}) \times 10^{-6}$ photons cm^{-2} s^{-1} keV^{-1}. A radial surface-brightness profile showed a clear excess of counts over extended emission at distances $< 1''$ from the core, and so we adopt the best-fitting model for the nuclear spectrum to be a single, unabsorbed, power law. We compared the results of my *Chandra* spectral fitting to a previously published *Chandra* analysis of 3C 338 (Di Matteo et al. 2001). These authors found an unabsorbed 1-keV flux density of $(7 \pm 2) \times 10^{-15}$ ergs cm^{-2} s^{-1} keV^{-1}, which is consistent with the value of $(10.6 \pm 2.8) \times 10^{-15}$ ergs cm^{-2} s^{-1} keV^{-1} that we measure (errors here are 1σ for one interesting parameter).

A.14. NGC 6251

The *Chandra* observation of the nucleus of NGC 6251 has already been analyzed in detail by us (Evans et al. 2005), and this paper should be consulted for a detailed description. Its nuclear spectrum is described by an absorbed power law of $N_{\rm H} = 4.5 \times 10^{20}$ atoms cm^{-2} and photon index $\Gamma = 1.67 \pm 0.06$, and is mixed with small-scale thermal emission of temperature $kT = 0.20 \pm 0.08$ keV, abundance 0.35 of solar, and normalization $(1.04^{+1.95}_{-0.48}) \times 10^{-4}$. Comparisons with other work are discussed by Evans et al. (2004).

A.15. 3C 388

An excess of counts at a position coincident with the nucleus is seen at energies of 3–7 keV, and the distribution of 3–7 keV counts is more point-like than an image created from 0.5–1 keV counts. This suggests that the nucleus is indeed detected, although there are relatively few counts. In order to provide some constraints on the nuclear emission of 3C 388, we adopted a spectral model consisting of an unabsorbed power law of photon index frozen at 2.0, together with thermal emission characterized by an Apec model of temperature and abundance frozen at 1.5 keV and 0.3 of solar, respectively. The thermal parameter values are consistent with those found from an analysis of the dependence of the hot-gas structure of 3C 388 as a function of the distance from the nucleus (Kraft et al., submitted). The fit

was good ($\chi^2 = 7.7$ for 9 dof), and the 1-keV unabsorbed flux density of the power law we measure with *Chandra* is 6±5 nJy. As an additional comparison with the other heavily absorbed FRII-type radio galaxies that we analyze in this paper, we measured the 1-keV unabsorbed flux density of the power law in a model fit consisting of an absorbed power law of $N_{\rm H} = 10^{23}$ atoms cm^{-2} and photon index frozen at 2.0, together with thermal emission. This value is 11 ± 6 nJy.

A.16. 3C 390.3

A model fit to a single, unabsorbed, power law of photon index 1.78 ± 0.09 provided a good fit to the nuclear spectrum ($\chi^2 = 24.86$ for 54 dof). No improvement in the fit was achieved with the inclusion of intrinsic absorption at the redshift of 3C 390.3: the best-fitting value of $N_{\rm H}$ was zero, with a 90% confidence upper limit of 2.6×10^{20} atoms cm^{-2}. Inspection of the χ^2 residuals of the best-fitting model showed slight positive residuals at energies ∼6–7 keV, which suggests that Fe Kα line-emission may be present, although its detection is not significant.

We measure the 2–10 keV unabsorbed luminosity of 3C 390.3 to be $\sim 3 \times 10^{44}$ ergs s^{-1}. Previous X-ray studies of 3C 390.3 show a range of 2–10 keV luminosities for this source: an *ASCA* observation (Sambruna et al. 1999) measured a photon index of 1.75 ± 0.02 and a 2–10 keV luminosity of $\sim 1 \times 10^{44}$ ergs s^{-1}, while long-term monitoring of the source with RXTE (Gliozzi et al. 2003) measured a photon index of 1.72 ± 0.02, and showed that the flux varies by a factor of over 2 on timescales of days.

A.17. 3C 449

A model fit consisting of an unabsorbed power law of photon index $2.14^{+0.25}_{-0.19}$ and a thermal (Apec) model of temperature $kT = 1.03 \pm 0.10$ provided a good fit to the spectrum ($\chi^2 = 37.5$ for 31 dof). The temperature of the gas is consistent with that measured by Croston et al. (2003). However, the 1-keV (aperture corrected) flux density of the nuclear power law measured with *XMM-Newton* is a factor of 2–3 higher than that measured with *Chandra*. Although we note that variability is a possible explanation for this effect, we decided to perform a further investigation by extracting a spectrum from the *Chandra* data using a source-centered circle of radius identical to that used for the *XMM-Newton* spectral extraction. A good fit was obtained to the *Chandra* spectrum with a model consisting of a power law and thermal emission, and the flux densities of the power law measured with

Chandra and *XMM-Newton* were consistent, and are also consistent with previously published *XMM-Newton* data (Donato et al. 2004). This highlights the importance of *Chandra* to our investigation, as its ability to separate spatially nuclear emission from unrelated (in this case thermal) emission is highly desirable.

A.18. 3C 452

Many spectral models were fitted to the data, but the only acceptable fit was found following Isobe et al. (2002) (who performed the original observation). This model fit consisted of a heavily absorbed power law [$N_{\rm H} = (5.7^{+0.9}_{-0.8}) \times 10^{23}$ atoms cm^{-2}; $\Gamma = 1.7$ (frozen)], a narrow 6.4-keV Fe Kα Gaussian emission line of equivalent width 160^{+180}_{-130} eV , reflection from a 'slab' of neutral material (such as the surface of an accretion disk or a torus), and thermal emission, characterized by an APEC model of temperature 0.63 ± 0.29 keV, abundance 0.4 of solar, and normalization $(2.84^{+20.06}_{-1.42}) \times 10^{-6}$. The fit was good: $\chi^2 = 65.9$ for 69 dof, and the parameter values we found are consistent with those measured by Isobe et al. (2002). No significant improvement to the fit was achieved with the addition of a second, unabsorbed power law of photon index frozen at 2. However, we note that the upper limit of the flux density of this unabsorbed component (which might be regarded as jet-related nuclear emission) is an interesting quantity.

A.19. 3C 465

A model fit consisting of a power law provided a poor fit to the nuclear spectrum, with strong residuals at $\lesssim$1 keV, clearly suggesting the presence of thermal emission on small scales. A good fit ($\chi^2 = 26.1$ for 24 dof) was achieved with the combination of an unabsorbed power law and a thermal (APEC) model. However, the photon index of the power law ($\Gamma = 1.19^{+0.26}_{-0.29}$) was surprisingly flat. Instead, a significant improvement in the fit ($\Delta\chi^2 = 3.9$ for one additional parameter) was achieved when the power law was allowed to have some intrinsic absorption. In this case, we measure the absorption to be $(4.4^{+6.0}_{-3.9}) \times 10^{21}$ atoms cm^{-2}, the photon index to be $1.86^{+0.72}_{-0.52}$, and the temperature of the thermal component to be $0.70^{+0.07}_{-0.06}$ keV (with abundance 0.3 of solar, and normalization $(4.51^{+0.90}_{-1.00}) \times 10^{-5}$). Models containing emission from a second power law instead of the thermal component failed to provide adequate descriptions of the spectrum. We compared the results of our analysis with previously published work (Hardcastle et al. 2005), and found all the spectral parameters to be consistent.

A.20. 3C 403

A model fit consisting of a heavily absorbed [$N_{\rm H} = 4.5^{+0.7}_{-0.6} \times 10^{23}$ atoms cm^{-2}] power law of photon index 1.76 ± 0.23, an unresolved Gaussian Fe Kα line and a second, unabsorbed, power law of photon index frozen at 2, provided a good fit to the data ($\chi^2 = 31.1$ for 50 dof). The addition of the Gaussian Fe Kα line is significant at 99.99% on an F-test. Thw equivalent width of this line is 220^{+60}_{-150} eV. The addition of a thermal APEC component did not significantly improve the fit ($\chi^2 = 29.0$ for 48 dof, with the probability of achieving a greater F by chance of 18.4%). We compared the results of the spectral fitting to previously published *Chandra* data (Kraft et al. 2005) and found all parameter values to be consistent.

A.21. 3C 405 (Cygnus A)

A good fit to the spectrum ($\chi^2 = 69.4$ for 84 dof) was achieved with the combination of a heavily absorbed [$N_{\rm H} = (1.7 \pm 0.3) \times 10^{23}$ atoms cm^{-2}] power law of photon index $\Gamma = 1.6 \pm 0.5$, a Gaussian Fe Kα line of equivalent width 250^{+210}_{-170} eV, and a second, unabsorbed, power law of photon index frozen at 2. The addition of a thermal component to this fit did not significantly improve the fit ($\Delta\chi^2 = 1.7$ for two additional parameters), with probability of achieving a greater F by chance of 36.4%. These best-fitting parameters are consistent with previously published work by Young et al. (2002), who used the same *Chandra* data.

A.22. Centaurus A

The nucleus of Centaurus A has been analyzed in detail by us (Evans et al. 2004), and this work should be consulted for a detailed description. The nuclear spectrum is well described by a heavily absorbed ($N_{\rm H} \sim 10^{23}$ atoms cm^{-2}) power law of photon index 1.7, accompanied by a narrow fluorescent Fe Kα emission line of equivalent width 60 ± 15 eV. In addition, Evans et al. (2004) find that a contribution from a softer power law, related to the parsec-scale VLBI jet, is necessary to model the nuclear continuum.

REFERENCES

Antonucci, R. 1993, ARA&A, 31, 473

Armitage, P. J. 2004, ASSL Vol. 308: Supermassive Black Holes in the Distant Universe, 89

Barthel, P. D., & Arnaud, K. A. 1996, MNRAS, 283, L45

Baum, S. A., Zirbel, E. L., & O'Dea, C. P. 1995, ApJ, 451, 88

Bettoni, D., Falomo, R., Fasano, G., & Govoni, F. 2003, A&A, 399, 869

Bicknell, G. V. 1994, ApJ, 422, 542

Bicknell, G. V. 1995, ApJS, 101, 29

Blandford, R. D., & Znajek, R. L. 1977, MNRAS, 179, 433

Blandford, R. D., & Begelman, M. C. 1999, MNRAS, 303, L1

Bohlin, R. C., Savage, B. D., & Drake, J. F. 1978, ApJ, 224, 132

Böhringer, H., et al. 2001, A&A, 365, L181

Bower, G. A., et al. 1998, ApJ, 492, L111

Canosa, C. M., Worrall, D. M., Hardcastle, M. J., & Birkinshaw, M. 1999, MNRAS, 310, 30

Cao, X., & Rawlings, S. 2004, MNRAS, 349, 1419

Capetti, A., Trussoni, E., Celotti, A., Feretti, L., & Chiaberge, M. 2002, New Astronomy Review, 46, 335

Chiaberge, M., Capetti, A., & Celotti, A. 1999, A&A, 349, 77

Chiaberge, M., Capetti, A., & Celotti, A. 2000, A&A, 355, 873

Chiaberge, M., Gilli, R., Capetti, A., & Macchetto, F. D. 2003, ApJ, 597, 166

Croston, J. H., Hardcastle, M. J., Birkinshaw, M., & Worrall, D. M. 2003, MNRAS, 346, 1041

Di Matteo, T., Johnstone, R. M., Allen, S. W., & Fabian, A. C. 2001, ApJ, 550, L19

Donato, D., Sambruna, R. M., & Gliozzi, M. 2004, ApJ, 617, 915

Elvis, M., et al. 1994, ApJS, 95, 1

Esin, A. A., McClintock, J. E., & Narayan, R. 1997, ApJ, 489, 865

Evans, D. A., Kraft, R. P., Worrall, D. M., Hardcastle, M. J., Jones, C., Forman, W. R., & Murray, S. S. 2004, ApJ, 612, 786

Evans, D. A., Hardcastle, M. J., Croston, J. H., Worrall, D. M., & Birkinshaw, M. 2005, MNRAS, 359, 363

Fabbiano, G., Trinchieri, G., Elvis, M., Miller, L., & Longair, M. 1984, ApJ, 277, 115

Falcke, H., Gopal-Krishna, & Biermann, P. L. 1995, A&A, 298, 395

Fanaroff, B. L., & Riley, J. M. 1974, MNRAS, 167, 31P

Ferrarese, L., & Ford, H. C. 1999, ApJ, 515, 583

Ferrarese, L., & Merritt, D. 2000, ApJ, 539, L9

Ford, H. C., et al. 1994, ApJ, 435, L27

Ghisellini, G., & Celotti, A. 2001, A&A, 379, L1

Giovannini, G., Cotton, W. D., Feretti, L., Lara, L., & Venturi, T. 2001, ApJ, 552, 508

Gliozzi, M., Sambruna, R. M., & Brandt, W. N. 2003, A&A, 408, 949

Gliozzi, M., Sambruna, R. M., & Eracleous, M. 2003, ApJ, 584, 176

Gliozzi, M., Sambruna, R. M., Brandt, W. N., Mushotzky, R., & Eracleous, M. 2004, A&A, 413, 139

Grandi, S. A., & Osterbrock, D. E. 1978, ApJ, 220, 783

Gopal-Krishna, & Wiita, P. J. 2000, A&A, 363, 507

Haas, M., et al. 2004, A&A, 424, 531

Hardcastle, M. J., & Worrall, D. M. 1999, MNRAS, 309, 969

Hardcastle, M. J., Birkinshaw, M., & Worrall, D. M. 2001, MNRAS, 326, 1499

Hardcastle, M. J., & Worrall, D. M. 2000, MNRAS, 314, 359

Hardcastle, M. J., Worrall, D. M., Birkinshaw, M., Laing, R. A., & Bridle, A. H. 2002, MNRAS, 334, 182

Hardcastle, M. J. 2004, A&A, 414, 927

Hardcastle, M. J., Worrall, D. M., Birkinshaw, M., Laing, R. A., & Bridle, A. H. 2005, MNRAS, 358, 843

Hardcastle, M. J., Sakelliou, I., & Worrall, D. M. 2005, MNRAS, 359, 1007

Harris, D. E., Finoguenov, A., Bridle, A. H., Hardcastle, M. J., & Laing, R. A. 2002, ApJ, 580, 110

Inda, M., et al. 1994, ApJ, 420, 143

Isobe, N., Tashiro, M., Makishima, K., Iyomoto, N., Suzuki, M., Murakami, M. M., Mori, M., & Abe, K. 2002, ApJ, 580, L111

Isobe, N., Makishima, K., Tashiro, M., & Hong, S. 2005, ApJ, 632, 781

Jackson, N., & Rawlings, S. 1997, MNRAS, 286, 241

Kraft, R. P., Vázquez, S. E., Forman, W. R., Jones, C., Murray, S. S., Hardcastle, M. J., Worrall, D. M., & Churazov, E. 2003, ApJ, 592, 129

Kraft, R. P., Hardcastle, M. J., Worrall, D. M., & Murray, S. S. 2005, ApJ, 622, 149

Kharb, P., & Shastri, P. 2004, A&A, 425, 825

Laing, R. A., Riley, J. M., & Longair, M. S. 1983, MNRAS, 204, 151

Laing, R. A., Jenkins, C. R., Wall, J. V., & Unger, S. W. 1994, ASP Conf. Ser. 54: The Physics of Active Galaxies, 54, 201

Lavalley, M., Isobe, T., & Feigelson, E. 1992, ASP Conf. Ser. 25: Astronomical Data Analysis Software and Systems I, 25, 245

Ledlow, M. J., & Owen, F. N. 1996, AJ, 112, 9

Leighly, K. M., O'Brien, P. T., Edelson, R., George, I. M., Malkan, M. A., Matsuoka, M., Mushotzky, R. F., & Peterson, B. M. 1997, ApJ, 483, 767

Marchesini, D., Celotti, A., & Ferrarese, L. 2004, MNRAS, 351, 733

Marconi, A., Capetti, A., Axon, D. J., Koekemoer, A., Macchetto, D., & Schreier, E. J. 2001, ApJ, 549, 915

Marshall, H. L., et al. 2005, ApJS, 156, 13

Merloni, A., Heinz, S., & di Matteo, T. 2003, MNRAS, 345, 1057

Müller, S. A. H., Haas, M., Siebenmorgen, R., Klaas, U., Meisenheimer, K., Chini, R., & Albrecht, M. 2004, A&A, 426, L29

Narayan, R., & Yi, I. 1995, ApJ, 452, 710

Pearson, T. J. 1996, ASP Conf. Ser. 100: Energy Transport in Radio Galaxies and Quasars, 100, 97

Pellegrini, S., Venturi, T., Comastri, A., Fabbiano, G., Fiore, F., Vignali, C., Morganti, R., & Trinchieri, G. 2003, ApJ, 585, 677

Owen, F. N., & Ledlow, M. J. 1994, ASP Conf. Ser. 54: The Physics of Active Galaxies, 54, 319

Protassov, R., van Dyk, D. A., Connors, A., Kashyap, V. L., & Siemiginowska, A. 2002, ApJ, 571, 545

Rawlings, S., & Saunders, R. 1991, Nature, 349, 138

Reynolds, C. S., di Matteo, T., Fabian, A. C., Hwang, U., & Canizares, C. R. 1996, MNRAS, 283, L111

Sambruna, R. M., Eracleous, M., & Mushotzky, R. F. 1999, ApJ, 526, 60

Sandage, A. 1973, ApJ, 183, 711

Shakura, N. I., & Sunyaev, R. A. 1973, A&A, 24, 337

Sun, M., Jerius, D., & Jones, C. 2005, ArXiv Astrophysics e-prints, arXiv:astro-ph/0501501

Tadhunter, C., Marconi, A., Axon, D., Wills, K., Robinson, T. G., & Jackson, N. 2003, MNRAS, 342, 861

Tadhunter, C. N., Morganti, R., di Serego-Alighieri, S., Fosbury, R. A. E., & Danziger, I. J. 1993, MNRAS, 263, 999

Turner, T. J., George, I. M., Nandra, K., & Mushotzky, R. F. 1997, ApJS, 113, 23

Urry, C. M., & Padovani, P. 1995, PASP, 107, 803

Wilson, A. S., & Yang, Y. 2002, ApJ, 568, 133

Worrall, D. M., & Birkinshaw, M. 1994, ApJ, 427, 134

Worrall, D. M., Birkinshaw, M., & Hardcastle, M. J. 2003, MNRAS, 343, L73

Wozniak, P. R., Zdziarski, A. A., Smith, D., Madejski, G. M., & Johnson, W. N. 1998, MNRAS, 299, 449

Young, A. J., Wilson, A. S., Terashima, Y., Arnaud, K. A., & Smith, D. A. 2002, ApJ, 564, 176

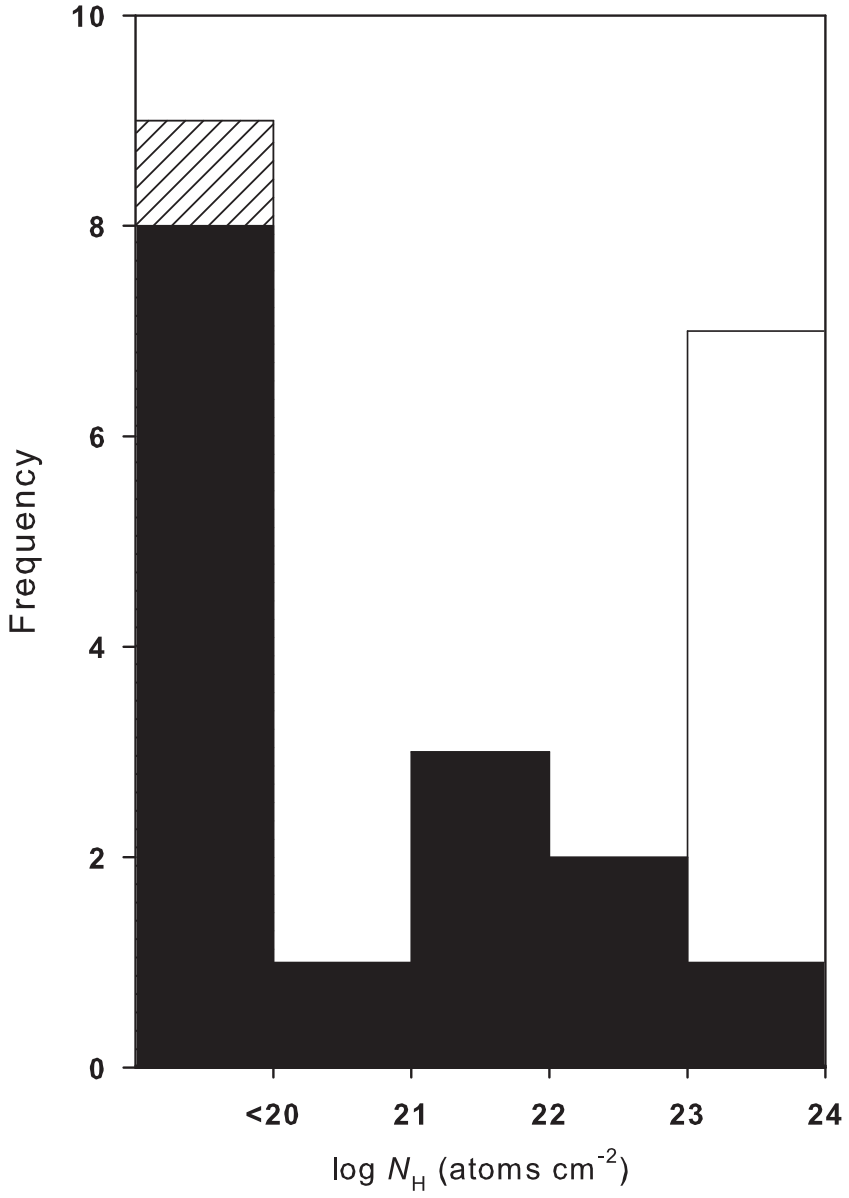

Fig. 1.— Histogram of the intrinsic absorption associated with the dominant component of X-ray emission in each of the sources. Black corresponds to the FRI-type sources; white corresponds to the FRII-type sources. The broad-line radio galaxy 3C 390.3 is (hatched box) distinguished from the other FRII-type sources.

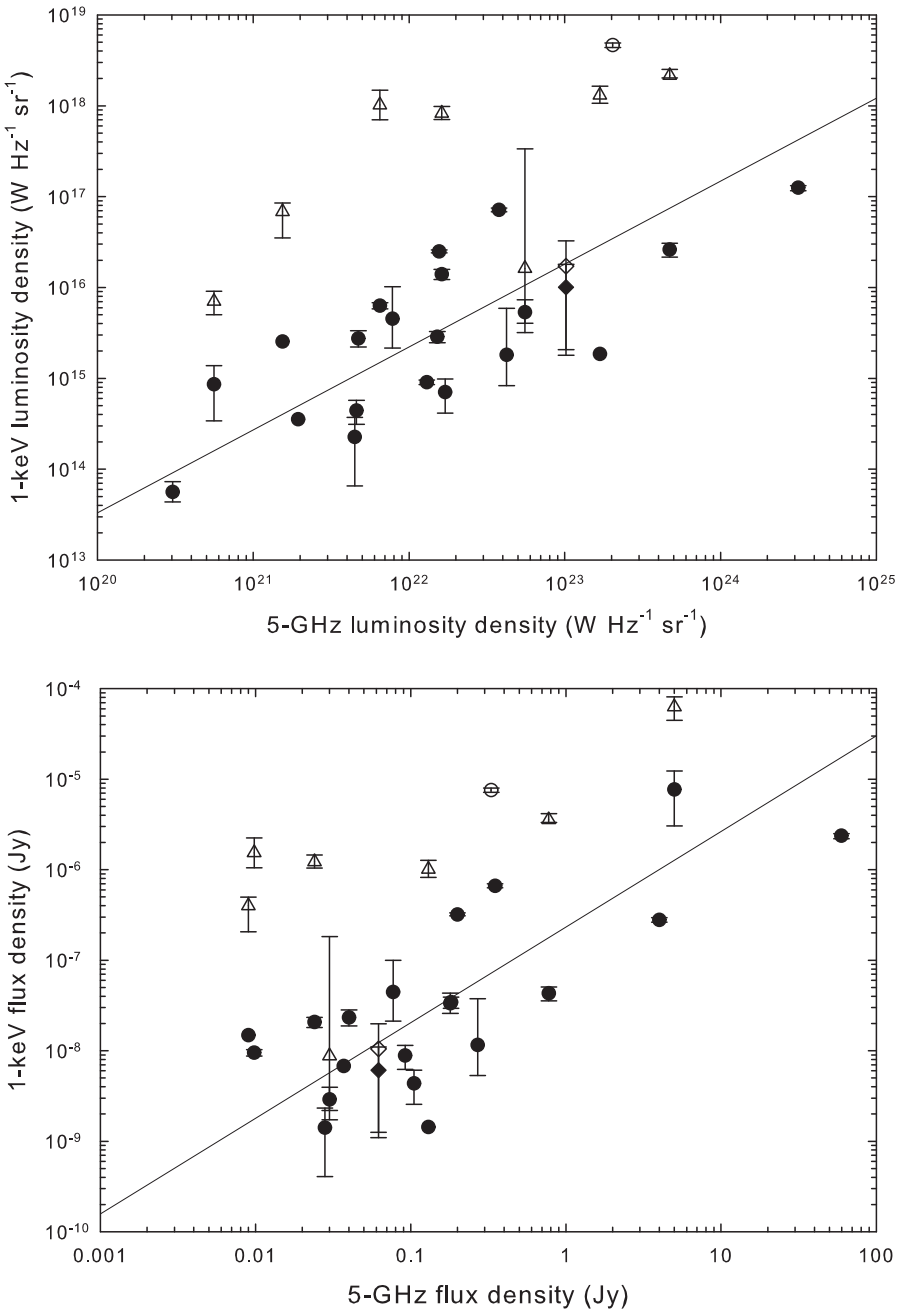

Fig. 2.— (a) (Upper panel) 1-keV unabsorbed X-ray luminosity density against 5-GHz radio core luminosity density for every component of X-ray emission. (b) (Lower panel) 1-keV unabsorbed X-ray flux density against 5-GHz radio core flux density for every component of X-ray emission. Filled circles correspond to those components with intrinsic absorption less than 5×10^{22} atoms cm^{-2}; hollow triangles represent those components with intrinsic absorption greater than 5×10^{22} atoms cm^{-2}. The hollow circle is the broad-line radio galaxy 3C 390.3, and the two diamonds represent the low-excitation FRII-type radio galaxy 3C 388 (see text for details). The line shown is the bisector of the two lines of best fit obtained by the Buckley-James regression of the 1-keV X-ray luminosity density (for components with $N_{\rm H} < 5 \times 10^{22}$ atoms cm^{-2}) and 5-GHz radio core luminosity density.

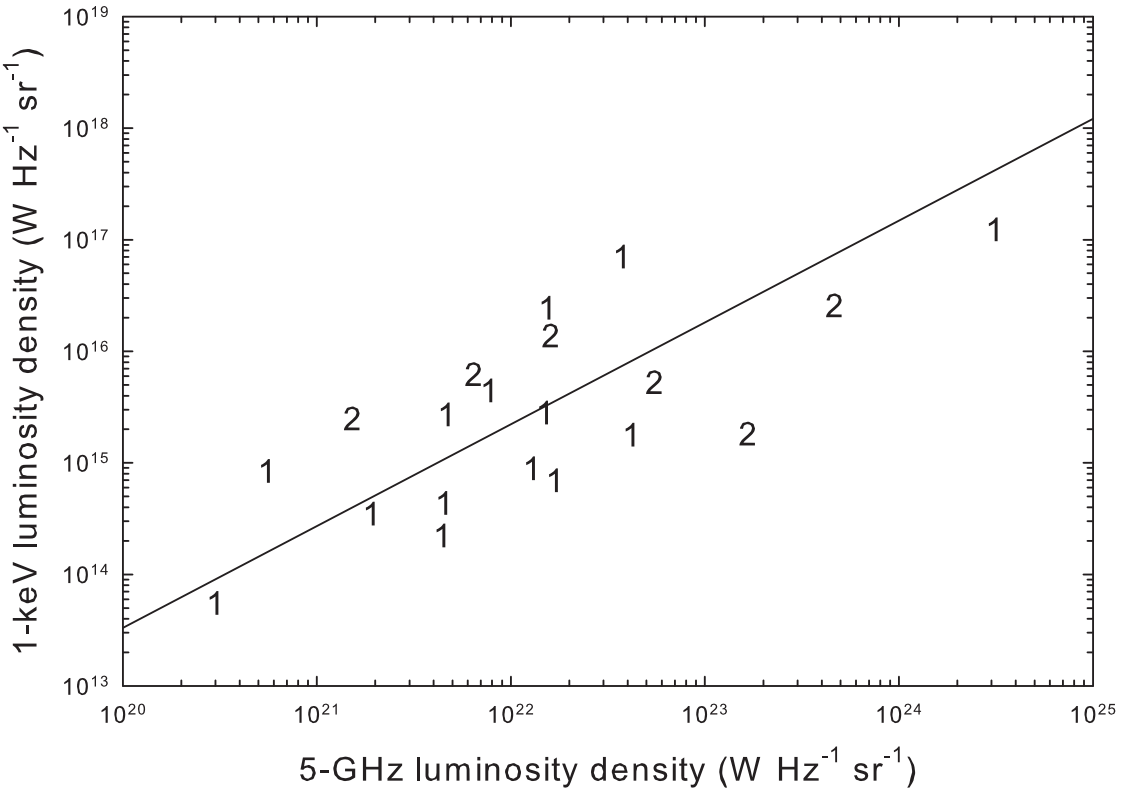

Fig. 3.— 1-keV unabsorbed X-ray luminosity density against 5-GHz radio core luminosity density for jet-related components of X-ray emission in FRI- and FRII-type sources. The observed X-ray and radio properties of the parsec-scale jets in FRI- and FRII-type radio galaxies are essentially indistinguishable.

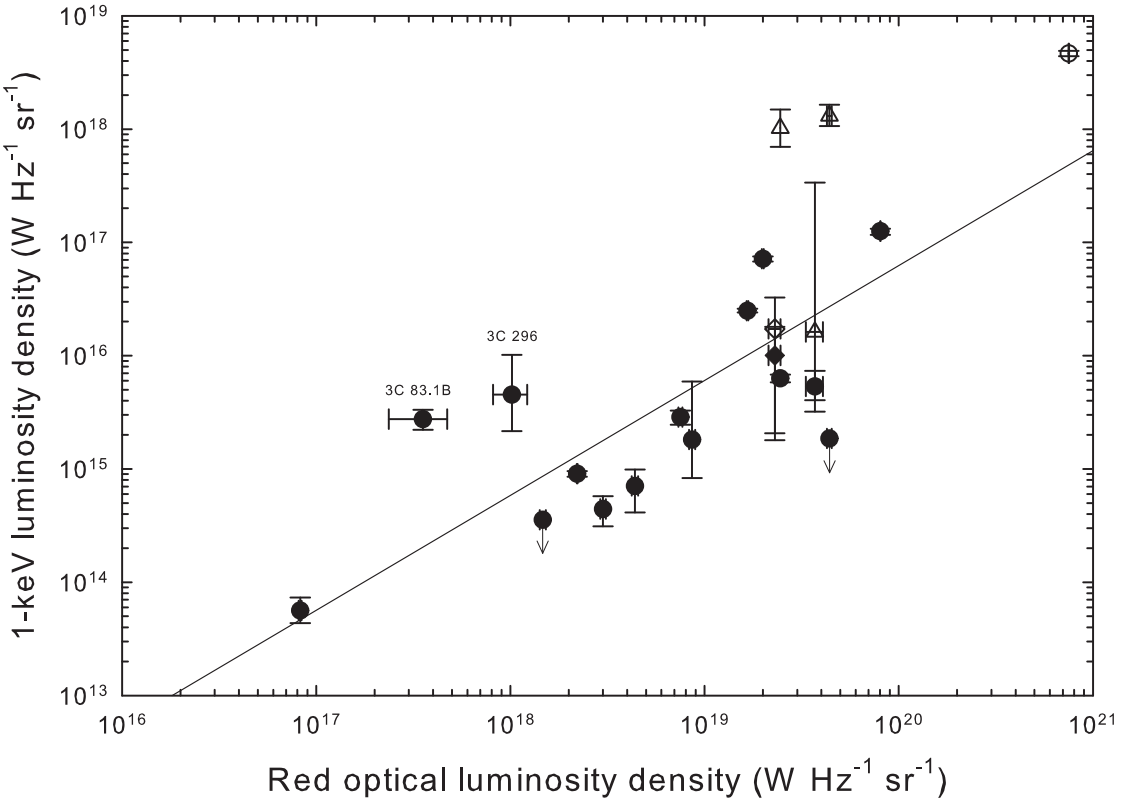

Fig. 4.— Red optical core luminosity density (mostly using the *HST* F702W filter) against 1-keV unabsorbed X-ray luminosity density for the components studied in this paper (where the data exist). Symbols are as in Figure 2.

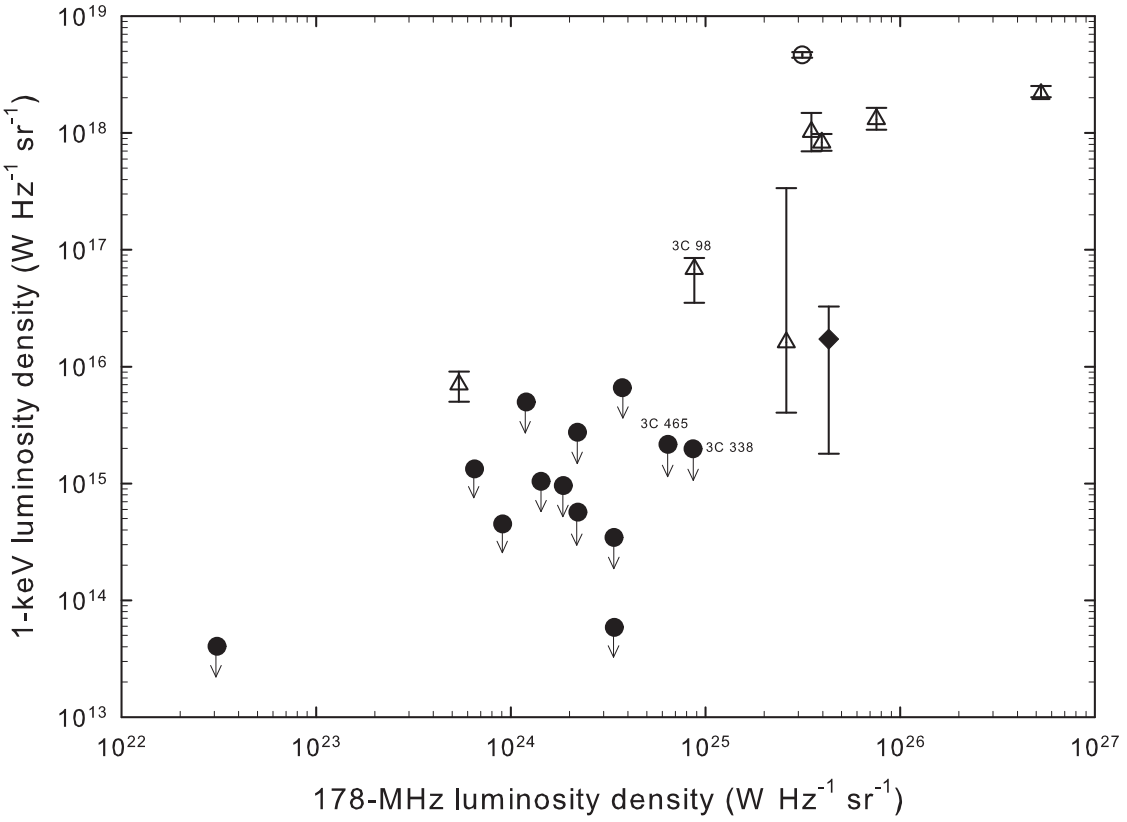

Fig. 5.— 1-keV unabsorbed luminosity density of the accretion-related components of the sources studied in this paper against 178-MHz luminosity density. Hollow triangles correspond to the accretion-related emission detected in the FRII-type sources and Cen A (the low-excitation radio galaxy 3C 388 is depicted with a filled diamond and the broad-line radio galaxy 3C 390.3 with a hollow circle). Filled circles correspond to the upper limits on the luminosity densities of 'hidden', accretion-related emission in the FRI-type sources, under the assumption that the accretion flow is obscured by a column of 10^{23} atoms cm^{-2}. Also highlighted are 3C 98, 3C 338, and 3C 465, the three sources which populate the FRI/FRII break in 178-MHz luminosity density.

Table 1: Overview of the main properties of the observed sources, ordered by 3C number.

Source	z	Galactic absorption (atoms cm^{-2})	FR class	RA (J2000)	DEC (J2000)	Optical Type	178-MHz luminosity (W Hz^{-1} sr^{-1})
3C 31	0.0167	5.41×10^{20}	1	01 07 24.96	+32 24 45.21	LERG	9.08×10^{23}
3C 33	0.0595	4.06×10^{20}	2	01 08 52.86	+13 20 13.80	NLRG	3.95×10^{25}
3C 66B	0.0215	8.91×10^{20}	1	02 23 11.41	+42 59 31.38	LERG	2.21×10^{24}
3C 83.1B (NGC 1265)	0.0255	1.45×10^{21}	1	03 18 15.86	+41 51 27.80	LERG	3.39×10^{24}
3C 84 (NGC 1275)	0.0177	1.45×10^{21}	1	03 19 48.16	+41 30 42.11	NLRG	3.74×10^{24}
3C 98	0.0306	1.29×10^{21}	2	03 58 54.43	+10 26 03.00	NLRG	8.75×10^{24}
3C 264	0.0208	2.45×10^{20}	1	11 45 05.01	+19 36 22.74	LERG	2.20×10^{24}
3C 272.1 (M84)	0.0029	2.78×10^{20}	1	12 25 03.74	+12 53 13.14	LERG	3.1×10^{22}
3C 274 (M87)	0.0041	2.54×10^{20}	1	12 30 49.42	+12 23 28.04	NLRG	3.4×10^{24}
3C 296	0.0237	1.86×10^{20}	1	14 16 52.94	+10 48 26.50	LERG	1.43×10^{24}
3C 321	0.0961	4.14×10^{20}	2	15 31 43.45	+24 04 19.10	NLRG	2.6×10^{25}
NGC 6109	0.0296	1.47×10^{20}	1	16 17 40.54	+35 00 15.10	LERG	1.86×10^{24}
3C 338	0.0303	8.90×10^{19}	1	16 28 38.48	+39 33 05.60	NLRG	8.63×10^{24}
NGC 6251	0.0244	5.82×10^{20}	1	16 32 31.97	+82 32 16.40	LERG	1.2×10^{24}
3C 388	0.0908	6.32×10^{20}	2	18 44 02.40	+45 33 29.70	LERG	4.29×10^{25}
3C 390.3	0.0569	4.16×10^{20}	2	18 42 08.99	+79 46 17.13	BLRG	3.14×10^{25}
3C 403	0.0590	1.54×10^{21}	2	19 52 15.80	+02 30 24.47	NLRG	3.5×10^{25}
3C 405	0.0565	3.06×10^{21}	2	19 59 28.36	+40 44 02.10	NLRG	4.90×10^{27}
3C 449	0.0171	1.19×10^{21}	1	22 31 20.90	+39 21 48.00	LERG	6.51×10^{23}
3C 452	0.0811	1.16×10^{21}	2	22 45 48.77	+39 41 15.70	NLRG	7.54×10^{25}
3C 465	0.0293	5.06×10^{20}	1	23 38 29.52	+27 01 55.90	LERG	6.41×10^{24}
Cen A	0.0008	7.69×10^{20}	1	13 25 27.62	-43 01 08.81	NLRG	5.4×10^{23}

Table 2. Observation log

Source (1)	Telescope (2)	Obs ID (3)	Instrument / Source CCD (4)	Observation Mode (5)	Nominal Exposure (ks) (6)	Screened Exposure (ks) (7)	Counts per frame (s^{-1}) (8)	Notes (9)
3C 31	*Chandra*	2147	ACIS-S3	FAINT	50	43.3	0.06	
3C 33	*XMM-Newton*	0203280301	EPIC	MEDIUM+MEDIUM+MEDIUM	7 (pn)	6.3 (pn)	1.20 (pn)	
3C 66B	*Chandra*	828	ACIS-S3	FAINT	50	29.6	0.06	
3C 83.1B	*Chandra*	3237	ACIS-S3	VFAINT	95	84.5	0.02	
3C 84	*XMM-Newton*	00085110101	EPIC	THIN+THIN+THIN	51 (pn)	24.7 (pn)	14.25 (pn)	
3C 98	*XMM-Newton*	0064600301	EPIC	THICK+THICK+MEDIUM	10 (pn)	3.2 (pn)	0.3 (pn)	
3C 264	*Chandra*	4916	ACIS-S3	FAINT	40	34.4	0.14	
3C 272.1	*Chandra*	803	ACIS-S3	VFAINT	30	28.1	0.09	
3C 274	*Chandra*	1808	ACIS-S3	FAINT	14	12.8	0.21	
3C 296	*Chandra*	3968	ACIS-S3	VFAINT	50	48.6	0.07	
3C 321	*Chandra*	3138	ACIS-S3	FAINT	50	46.6	0.04	
NGC 6109	*Chandra*	3985	ACIS-S3	VFAINT	20	19.0	0.02	
3C 338	*Chandra*	497	ACIS-S3	FAINT	20	18.3	0.05	
NGC 6251	*Chandra*	4130	ACIS-I3	VFAINT	50	43.0	0.36	See Evans et al. (2005)
3C 388	*Chandra*	5295	ACIS-I3	VFAINT	33	30.7	0.02	
3C 390.3	*Chandra*	830	ACIS-S3	FAINT	35	23.9	–	Readout streak
3C 403	*Chandra*	2968	ACIS-S3	FAINT	50	45.9	0.14	See Kraft et al. (2005)
3C 405	*Chandra*	1707	ACIS-S3	VFAINT	10	9.2	0.06	
3C 449	*Chandra*	4057	ACIS-S3	VFAINT	30	24.7	0.035	
3C 449	*XMM-Newton*	0002970101	EPIC	MEDIUM+MEDIUM+MEDIUM	18.5 (pn)	16.7 (pn)	0.35 (pn)	
3C 452	*Chandra*	2195	ACIS-S3	FAINT	80	79.5	0.09	
3C 465	*Chandra*	4816	ACIS-S3	VFAINT	50	49.3	0.02	
3C 465	*XMM-Newton*	0002960101	EPIC	MEDIUM+MEDIUM+MEDIUM	9.7 (pn)	7.8 (pn)	0.85 (pn)	
Cen A	*Chandra*	1600/1601	HETGS	FAINT	100	98.3	–	See Evans et al. (2004)
Cen A	*XMM-Newton*	0093650201	EPIC	MEDIUM+MEDIUM+MEDIUM	19.3 (pn)	16.8 (pn)	15 (pn)	See Evans et al. (2004)
Cen A	*XMM-Newton*	0093650301	EPIC	MEDIUM+MEDIUM+MEDIUM	9.3 (pn)	7.9 (pn)	15 (pn)	See Evans et al. (2004)

Note. — Col. (1): Name of source. Col. (2): Telescope used to perform observation. Col. (3): Observation ID. Col. (4): Instrument / CCD source located on. Col. (5): Observation mode. Indicates data mode for *Chandra* and optical blocking filter for *XMM-Newton* MOS1, MOS2, and pn cameras. Col. (6): Nominal exposure time. Col. (7): Screened exposure time. Col. (8): Point source counts per frame time. Used as a pileup diagnostic. Col. (9): Additional remarks.

Table 3. Main spectral parameters of the $z < 0.1$ radio-galaxy nuclei

Source (1)	Telescope (2)	Description of best spectrum (3)	$N_{\rm H}$ (atoms cm^{-2}) (4)	Γ (5)	E (keV) (6)	σ (keV) (7)	kT (keV) (8)	$L_{(2-10{\rm keV})}$ (Power Law) (ergs s^{-1}) (9)	χ^2/dof (10)	Comments (11)
3C 31	C	PL+TH	–	$1.48^{+0.28}_{-0.32}$	–	–	$0.68^{+0.08}_{-0.07}$	4.7×10^{40}	9.6/25	–
3C 33	X	$N_{\rm H}$(PL+Gauss)+PL	$(3.9^{+0.7}_{-0.6})\times10^{23}$	$\Gamma_1 = 1.7$ (f);	6.42 ± 0.09	0.1 (f)	–	6.3×10^{43}	49.0/39	–
			–	$\Gamma_2 = 1.7$ (f)				1.7×10^{42}		
3C 66B	C	PL+TH	–	2.03 ± 0.18	–	–	$0.41^{+0.23}_{-0.10}$	1.3×10^{41}	29.1/34	
3C 83.1B	C	$N_{\rm H}$(PL)+TH	$(3.2^{+0.8}_{-0.7})\times10^{22}$	$2.00^{+0.27}_{-0.20}$	–	–	$0.58^{+0.15}_{-0.14}$	1.3×10^{41}	9.5/12	
3C 84	X	PL+Gauss+TH+TH	–	1.81 ± 0.03	$6.39^{+0.08}_{-0.09}$	0.01 (f)	$kT_1 = 0.77 \pm 0.04$;	8.2×10^{42}	1156.0/1151	
							$kT_2 = 2.74 \pm 0.10$			
3C 98	X	$N_{\rm H}$ (PL+Gauss)+TH	$(1.2^{+0.3}_{-0.2})\times10^{23}$	$1.68^{+0.23}_{-0.37}$	6.37 ± 0.10	0.1 (f)	0.98 ± 0.12	5.4×10^{42}	32.8/40	
3C 264	C	PL	–	$2.34^{+0.07}_{-0.08}$	–	–	–	7.5×10^{41}	123.0/147	
3C 272.1	C	$N_{\rm H}$(PL)	$(1.9^{+0.8}_{-0.7})\times10^{21}$	$2.14^{+0.34}_{-0.30}$	–	–	–	2.2×10^{39}	11.3/24	
3C 274	C	PL+TH	–	2.09 ± 0.06	–	–	$0.75^{+0.17}_{-0.14}$	3.9×10^{40}	84.2/98	
3C 296	C	$N_{\rm H}$ (PL)+TH	$(1.5 \pm 0.9)\times10^{22}$	$1.77^{+0.60}_{-0.52}$	–	–	$0.75^{+0.27}_{-0.46}$	3.1×10^{41}	9.3/21	
3C 321	C	$N_{\rm H}$(PL+Gauss)+PL+TH	$(1.5^{+9.6}_{-0.9})\times10^{23}$	$\Gamma_1 = 1.7$ (f);	6.40 (f)	0.5 (f)	0.49 ± 0.15	$(1.2^{+24.3}_{-0.9})\times10^{42}$	9.8/8	
			–	$\Gamma_2 = 2$ (f)				$(2.6^{+1.0}_{-1.1})\times10^{41}$		
NGC 6109	C	PL+TH	–	1.47 ± 0.47	–	–	$0.63^{+0.14}_{-0.17}$	2.3×10^{40}	1.5/6	
3C 338	C	PL	–	2.37 ± 0.81	–	–	–	2.0×10^{40}	4.5/3	
NGC 6251	C	$N_{\rm H}$(PL)+TH	4.5×10^{20} (f)	1.67 ± 0.06	–	–	0.20 ± 0.08	5.9×10^{42}	107/134	
3C 388	C	PL+TH	–	2 (f)	–	–	1.03 ± 0.29	4.9×10^{41}	6.4/8	
3C 390.3	C	PL	–	1.78 ± 0.09	–	–	–	3.2×10^{44}	24.9/54	Tentative Fe Kα
3C 449	C	PL	–	$1.67^{+0.45}_{-0.49}$	–	–	–	$<2.9\times10^{40}$	8.8/4	Upper limits
3C 403	C	$N_{\rm H}$(PL+Gauss)+PL	$(4.5^{+0.7}_{-0.6})\times10^{23}$	$\Gamma_1 = 1.76 \pm 0.23$;	6.32 ± 0.02	0.1 (f)	–	7.1×10^{43}	31.1/50	–
			–	$\Gamma_2 = 2$ (f)				3.1×10^{41}		
3C 405	C	$N_{\rm H}$(PL+Gauss)+PL	$(1.7^{+0.4}_{-0.3})\times10^{23}$	$\Gamma_1 = 1.60^{+0.53}_{-0.54}$;	6.41 ± 0.04	0.1 (f)	–	1.9×10^{44}	69.4/84	–
			–	$\Gamma_2 = 2$ (f)				1.3×10^{42}		
3C 452	C	$N_{\rm H}$(PL+Gauss)+PEXRAV+TH	$(5.7^{+0.9}_{-0.8})\times10^{23}$	1.7 (f)	6.4 (f)	0.1 (f)	0.63 ± 0.29	1.0×10^{44}	65.9/69	Follows Isobe et
3C 465	C	$N_{\rm H}$(PL)+TH	$(4.5^{+6.0}_{-3.9})\times10^{21}$	$1.86^{+0.72}_{-0.52}$	–	–	$0.70^{+0.07}_{-0.06}$	1.1×10^{41}	22.2/23	
Cen A	C/X	$N_{\rm H}$(PL+Gauss)+$N_{\rm H}$(PL)	$N_{\rm H,1} = (1.2 \pm 0.2)\times10^{23}$	$\Gamma_1 = 1.72 \pm 0.21$;	6.40 ± 0.01	0.02 ± 0.01	–	$\sim 5\times10^{41}$	–	See Evans et al.
			$N_{\rm H,2} = (3.8 \pm 2.0)\times10^{22}$	$\Gamma_2 = 2$ (f)				2.8×10^{37}		

Note. — Col. (1): Name of source. Col. (2): Telescope used (C=*Chandra*, X=*XMM-Newton*). Col. (3): Description of best spectrum ($N_{\rm H}$=Intrinsic absorption, PL=Power Law, Gauss=Redshifted Gaussian Line, TH=T PEXRAV=Reflection from neutral material. Col. (4): Intrinsic neutral hydrogen column density. Galactic absorption has also been applied (see Table 1 for values). Col. (5): Power-law photon index. Col. (6): Gaussian energy. Col. (7): Gaussian linewidth. Col. (8): Thermal temperature. Col. (9): 2–10 keV unabsorbed luminosity of primary power law. Col. (10): Value of χ^2 and degrees of freedom. Col. (11): Comments. (f): In parameter was frozen.

Table 4. X-ray, radio, and optical flux and luminosity densities

Source (1)	$N_{\rm H}$ (atoms cm^{-2}) (2)	1-keV flux density (nJy) (3)	5-GHz VLA flux density (Jy) (4)	HST flux density (μJy) (5)	1-keV luminosity density (W Hz^{-1} s^{-1}r) (6)	5-GHz VLA luminosity density (W Hz^{-1} sr^{-1}) (7)	HST luminosity density (W Hz^{-1} sr^{-1}) (8)	HST Reference (9)
3C 31	–	8.9 ± 2.6	0.09	60 ± 2	$(4.4 \pm 1.3) \times 10^{14}$	4.60×10^{21}	$(3.0 \pm 0.1) \times 10^{18}$	HW00
3C 33	$(3.9^{+0.7}_{-0.6}) \times 10^{23}$	1200 ± 200	0.02*	–	$(8.3^{+1.5}_{-1.3}) \times 10^{17}$	1.62×10^{22}*	–	–
	–	21 ± 3			$(1.4 \pm 0.2) \times 10^{16}$			
3C 66B	–	34 ± 5	0.18	90 ± 2	$(2.9 \pm 0.4) \times 10^{15}$	1.52×10^{22}	$(7.5 \pm 0.2) \times 10^{18}$	HW00
3C 83.1B	$(3.2^{+0.8}_{-0.7}) \times 10^{22}$	23 ± 5	0.04	3 ± 1	$(2.8^{+0.6}_{-0.5}) \times 10^{15}$	4.72×10^{21}	$(3.5 \pm 1.2) \times 10^{17}$	HW00
3C 84	–	2400^{+100}_{-200}	59.60	1500 ± 10	$(1.3 \pm 0.1) \times 10^{17}$	3.15×10^{24}	$(8.0 \pm 0.01) \times 10^{19}$	HW00
3C 98	$(1.2^{+0.3}_{-0.2}) \times 10^{23}$	400^{+100}_{-190}	0.01*	–	$(6.9^{+1.7}_{-3.3}) \times 10^{16}$	1.54×10^{21}*	–	–
	–	< 15 (fs)			$< 2.5 \times 10^{15}$ (fs)			
3C 264	–	320 ± 10	0.20	210 ± 2	$(2.5^{+0.1}_{-0.8}) \times 10^{16}$	1.56×10^{22}	$(1.7 \pm 0.02) \times 10^{19}$	HW00
3C 272.1	$(1.9^{+0.8}_{-0.7}) \times 10^{21}$	33^{+10}_{-8}	0.18	49 ± 1	$(5.6^{+1.7}_{-1.3}) \times 10^{13}$	3.04×10^{20}	$(8.3 \pm 0.2) \times 10^{16}$	HW00
3C 274	–	280 ± 20	4	680 ± 2	$(9.1 \pm 0.5) \times 10^{14}$	1.30×10^{22}	$(2.2 \pm 0.01) \times 10^{18}$	HW00
3C 296	$(1.5 \pm 0.9) \times 10^{22}$	45^{+56}_{-23}	0.08	10 ± 2	$(4.5^{+5.6}_{-2.4}) \times 10^{15}$	7.83×10^{21}	$(1.0 \pm 0.2) \times 10^{18}$	HW00
3C 321	$(1.5^{+9.6}_{-0.9}) \times 10^{23}$	$8.8^{+174}_{-6.6}$	0.03*	20 ± 2*	$(1.6^{+32}_{-1.2}) \times 10^{16}$	5.55×10^{22}*	$(3.7 \pm 0.4) \times 10^{19}$*	SH04
	–	$2.9^{+1.1}_{-1.2}$			$(5.4^{+2.0}_{-2.2}) \times 10^{15}$			
NGC 6109	–	$1.4^{+0.9}_{-1.0}$	0.03	–	$(2.3^{+1.5}_{-1.6}) \times 10^{14}$	4.5×10^{21}	–	–
3C 338	–	$4.4^{+1.7}_{-1.8}$	0.11	27 ± 1	$(7.1^{+2.8}_{-2.9}) \times 10^{14}$	1.70×10^{22}	$(4.4 \pm 0.2) \times 10^{18}$	HW00
NGC 6251	4.5×10^{20} (f)	660 ± 30	0.35	190 ± 2	$(7.2 \pm 0.04) \times 10^{16}$	3.78×10^{22}	$(2.0 \pm 0.02) \times 10^{19}$	Evans et al. (2005)
3C 388	–	6.1 ± 4.9	0.06	14 ± 1	$(1.0 \pm 0.8) \times 10^{16}$	1.0×10^{23}	$(2.3 \pm 0.2) \times 10^{19}$	SH04
3C 390.3	–	7600 ± 400	0.33	1200 ± 10	$(4.7 \pm 0.3) \times 10^{18}$	2.30×10^{23}	$(7.5 \pm 0.2) \times 10^{20}$	HW00
3C 403	$(4.5^{+0.7}_{-0.6}) \times 10^{23}$	1500^{+700}_{-500}	9.8×10^{-3}*	37*	$(1.0^{+0.5}_{-0.3}) \times 10^{18}$	6.50×10^{21}*	2.5×10^{19}*	KS04
	–	9.5 ± 0.8			$(6.3 \pm 0.5) \times 10^{15}$			
3C 405	$(1.7^{+0.4}_{-0.3}) \times 10^{23}$	3600^{+600}_{-200}	0.78*	–	$(2.2^{+0.4}_{-0.1}) \times 10^{18}$	4.7×10^{23}*	–	–
	–	43 ± 8			$(2.6 \pm 0.5) \times 10^{16}$			
3C 449	–	< 6.8	0.04	28 ± 1	$< 3.6 \times 10^{14}$	1.94×10^{21}	$(1.5 \pm 0.05) \times 10^{18}$	HW00
3C 452	$(5.7^{+0.9}_{-0.8}) \times 10^{23}$	1000^{+300}_{-200}	0.13*	34 ± 1*	$(1.31 \pm 0.3) \times 10^{18}$	1.68×10^{23}*	$(4.4 \pm 0.1) \times 10^{19}$*	SH04
	–	< 1.44 (fs)		–	$< 1.86 \times 10^{15}$ (fs)			
3C 465	$(4.5^{+6.0}_{-3.9}) \times 10^{21}$	12^{+26}_{-6}	0.27	55 ± 2	$(1.8^{+4.1}_{-1.0}) \times 10^{15}$	4.23×10^{22}	$(8.6 \pm 0.3) \times 10^{18}$	HW00
Cen A	$(1.2 \pm 0.1) \times 10^{23}$	63000 ± 18000	5*	–	$(7.1 \pm 2.0) \times 10^{15}$	5.60×10^{20}*	–	–
	$(3.6^{+2.2}_{-2.3}) \times 10^{22}$	7700 ± 4600			$(8.6 \pm 5.2) \times 10^{14}$			

*Radio/optical flux/luminosity density quoted is total and is not implicitly associated with this component of X-ray emission

Note. — Col. (1): Name of source. Col. (2): Intrinsic absorption of X-ray component. Col. (3): 1-keV unabsorbed flux density of X-ray component. Col. (4): 5-GHz VLA flux density of core. Col. (5): Red *HST* flux density (dereddened for Milky Way). Mostly uses data from the F702W filter. Col. (6): 1-keV unabsorbed luminosity density of X-ray component. Col. (7): 5-GHz VLA luminosity density of core. Taken from the online 3CRR catalogue (http://www.3crr.dyndns.org/) and references therein. Col. (8): Red *HST* luminosity density (dereddened for Milky Way). Mostly uses data from the F702W filter. Col. (9): Reference used for HST data (HW00=Hardcastle & Worrall (2000), KS04=Kharb & Shastri (2004), SH04=O. Shorttle, private communication. (fs): Upper limit to soft, unabsorbed X-ray emission in heavily absorbed sources (not statistically required).

Table 5: Black hole masses, and unabsorbed X-ray and Eddington luminosities and efficiencies for components with $N_{\rm H} > 5 \times 10^{22}$ atoms cm^{-2} plus the BLRG 3C 390.3

Source	log $M_{\rm BH}$ ($M_\odot$)	$L_{\rm Edd}$ (ergs s^{-1})	$L_{0.5-10{\rm keV}}$ (ergs s^{-1})	$\eta_{\rm X,Edd}$
3C 33	8.68	6.2×10^{46}	9.7×10^{43}	1.6×10^{-3}
3C 98	8.23	2.2×10^{46}	8.2×10^{42}	3.7×10^{-4}
3C 390.3	8.53	4.4×10^{46}	5.0×10^{44}	1.1×10^{-2}
3C 403	8.41	3.3×10^{46}	1.1×10^{44}	3.3×10^{-3}
3C 405	9.40	3.3×10^{47}	2.8×10^{44}	8.5×10^{-4}
3C 452	8.54	4.5×10^{46}	1.5×10^{44}	3.3×10^{-3}
Cen A	8.30	2.6×10^{46}	7.8×10^{41}	3.0×10^{-5}

Table 6. 90%-confidence upper limits to hidden accretion-related emission in likely jet-dominated FRI-type radio-galaxy nuclei, assuming obscuring columns of either 10^{23} atoms cm^{-2} or 10^{24} atoms cm^{-2}. Shown are the black hole masses, unabsorbed 0.5–10 keV X-ray and Eddington luminosities, and efficiencies.

			$N_{\rm H} = 10^{23}$ atoms cm^{-2}		$N_{\rm H} = 10^{24}$ atoms cm^{-2}	
Source	log $M_{\rm BH}$ ($M_\odot$)	$L_{\rm Edd}$ (ergs s^{-1})	$L_{0.5-10{\rm keV}}$ (ergs s^{-1})	$\eta_{\rm X,Edd}$	$L_{0.5-10{\rm keV}}$ (ergs s^{-1})	$\eta_{\rm X,Edd}$
3C 31	7.89	1.0×10^{46}	$<5.4\times10^{40}$	$<5.4\times10^{-6}$	$<2.0\times10^{42}$	$<2.0\times10^{-4}$
3C 66B	8.84	9.0×10^{46}	$<6.7\times10^{40}$	$<7.4\times10^{-7}$	$<4.0\times10^{42}$	$<4.4\times10^{-5}$
3C 83.1B	9.01	1.3×10^{47}	$<4.1\times10^{40}$	$<3.1\times10^{-7}$	$<8.8\times10^{41}$	$<6.8\times10^{-6}$
3C 84	9.28	2.5×10^{47}	$<7.8\times10^{41}$	$<3.1\times10^{-6}$	$<2.3\times10^{42}$	$<9.2\times10^{-6}$
3C 264	8.85	9.2×10^{46}	$<3.3\times10^{41}$	$<3.6\times10^{-6}$	$<1.7\times10^{42}$	$<1.8\times10^{-5}$
3C 272.1	9.18	1.9×10^{47}	$<4.8\times10^{39}$	$<2.5\times10^{-8}$	$<1.6\times10^{41}$	$<8.5\times10^{-7}$
3C 274	9.38	3.0×10^{47}	$<7.0\times10^{39}$	$<2.3\times10^{-8}$	$<1.3\times10^{41}$	$<4.3\times10^{-7}$
3C 296	9.13	1.8×10^{47}	$<1.2\times10^{41}$	$<6.8\times10^{-7}$	$<2.1\times10^{42}$	$<1.2\times10^{-5}$
NGC 6109	–	–	$<1.1\times10^{41}$	–	$<2.1\times10^{42}$	–
3C 338	9.23	2.2×10^{47}	$<2.3\times10^{41}$	$<1.0\times10^{-6}$	$<4.4\times10^{42}$	$<2.0\times10^{-5}$
NGC 6251	8.78	7.8×10^{46}	$<5.9\times10^{41}$	$<7.6\times10^{-6}$	$<1.6\times10^{43}$	$<2.0\times10^{-4}$
3C 449	7.71	6.7×10^{45}	$<1.6\times10^{41}$	$<2.4\times10^{-5}$	$<4.7\times10^{43}$	$<7.0\times10^{-3}$
3C 465	9.32	2.7×10^{47}	$<2.6\times10^{41}$	$<9.6\times10^{-7}$	$<5.9\times10^{43}$	$<2.2\times10^{-4}$